Compton Sources of Electromagnetic Radiation*

Geoffrey A. Krafft
Jefferson Lab, Old Dominion University
Gerd Priebe
Max Born Institute
(With some intro slides from Todd Satogata)

*Reviews of Accelerator Science and Technology, **3**, 147 (2010)

Outline

- Basic Physics
  - Compton Effect
  - Energy
  - Flux
  - Energy Spread
  - Pulse Length
  - Brilliance
  - Harmonics/ Broadening
- Laser Performance
  - Self-Excited Arrangements
  - External High Power Optical Cavities
  - High Peak Power

- Ring Sources
  - Direct Illumination
  - Self Excited
  - External Cavities
- Linac/ERL Based Sources
  - Self Excited
  - Direct Illumination
- Future Proposals
  - X-Rays
  - Gamma-Rays
- Conclusions

Compton Effect

TABLE I

Wave-length of Primary and Scattered γ-rays

	Angle	μ/ρ	τ/ρ	λ obs.	λ calc.
Primary	0°	.076	.017	0.022 A	(0.022 A)
Scattered	45°	.10	.042	.030	0.029
"	90°	.21	.123	.043	0.047
"	135°	.59	.502	.068	0.063

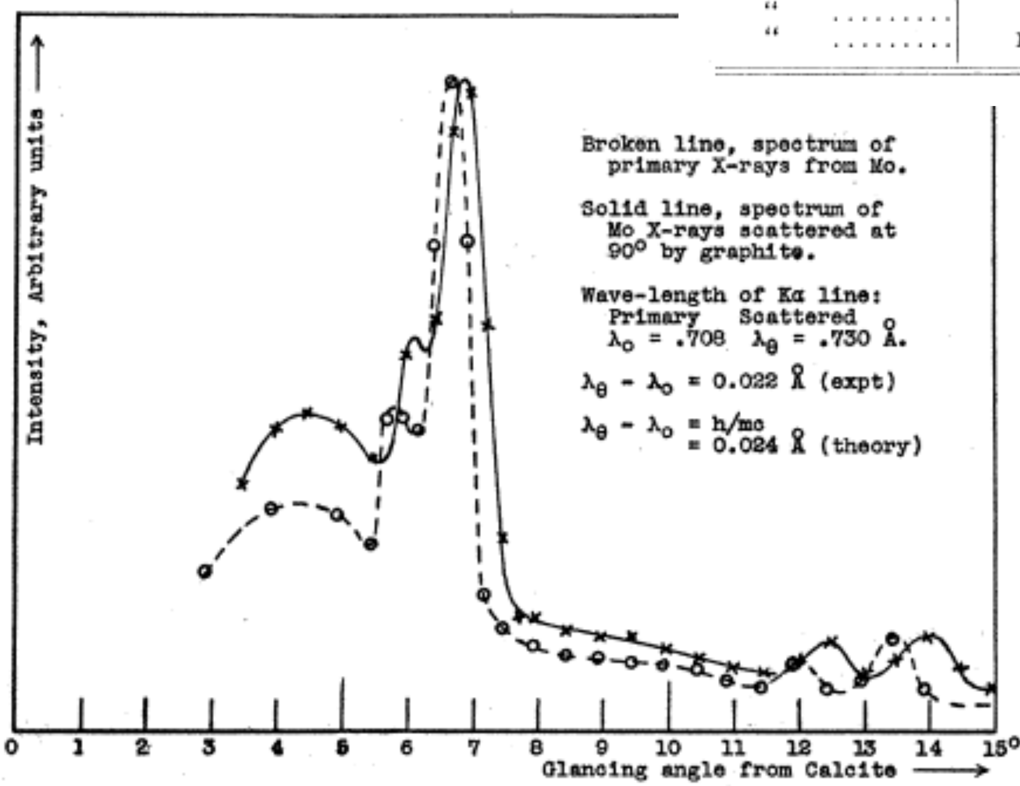

Fig. 4. Spectrum of molybdenum X-rays scattered by graphite, compared with the spectrum of the primary X-rays, showing an increase in wave-length on scattering.

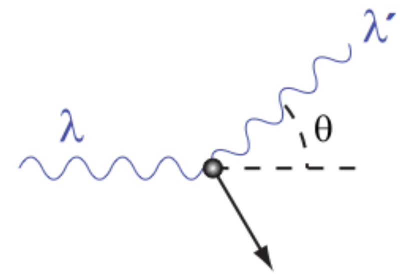

A. H. Compton, Phys. Rev., 21, 483 (1923)

Proved light had particle-like properties when observed with low intensity light

Nobel prize in Physics, 1927!!

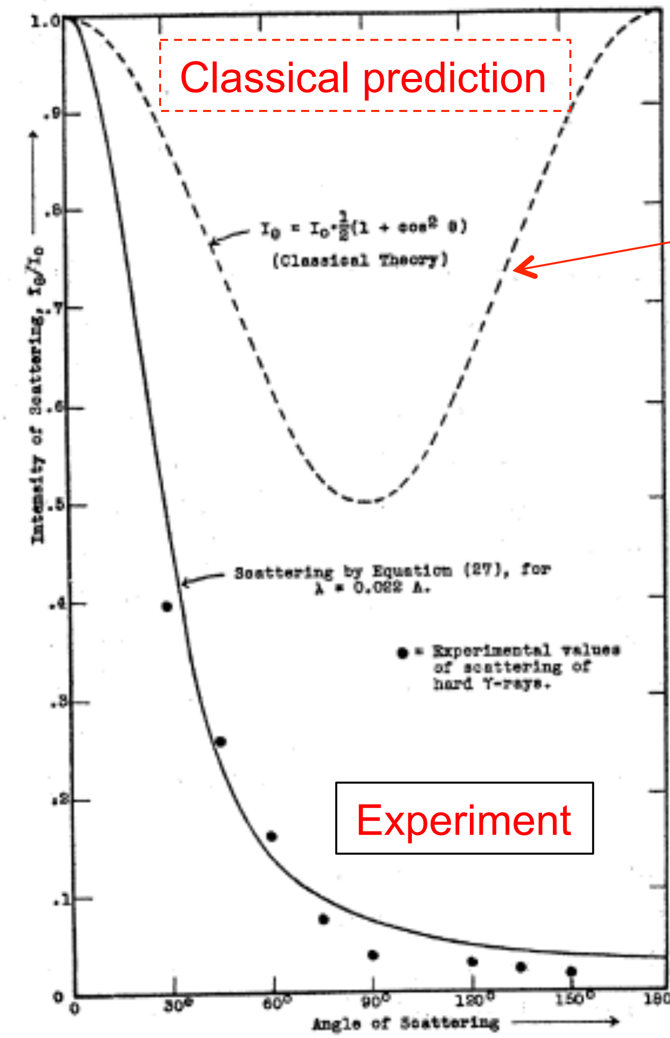

Fig. 7. Comparison of experimental and theoretical intensities of scattered γ-rays.

Unpolarized Incident X-ray Beam

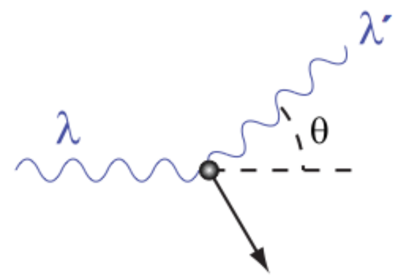

$$\lambda' - \lambda = \frac{h}{m_e c}(1 - \cos\theta)$$

Planar scattering
Quantum effect!

Undulators/Wigglers vs Compton

- Undulators and wigglers get small wavelength light from high-energy (expensive, multi-GeV) electrons

$$\lambda = \frac{\lambda_{\mathrm{undulator}}}{2\gamma^2}\left(1 + \frac{\kappa^2}{2}\right) \qquad \kappa = \frac{eB\lambda_{\mathrm{undulator}}}{2\pi m_e c}$$

Deflection parameter

- Synchrotron light sources:

$$\gamma \approx \text{ thousands} \qquad \kappa \approx \sqrt{2} \ \text{(undulators)}, \quad \approx \text{tens} \ \text{(wigglers)}$$

- Compton sources use a high-powered laser to generate EM fields instead of wigglers or undulators
  - Scattered photons from laser are shifted into X-ray

$$\lambda = \frac{\lambda_{\mathrm{laser}}}{4\gamma^2}\left(1 + \frac{\kappa^2}{2}\right)$$

$$\lambda_{\mathrm{laser}} \approx 10^{-4}\lambda_{\mathrm{undulator}} \qquad \Rightarrow \qquad \text{lower } \gamma \text{ by } \approx 10^2$$

Big deal!!Tens of MeV electrons!

A Recent Paper

The first demonstration of this concept was reported by Carmel *et al* [12] at Naval Research Laboratory. In this demonstration, x-rays were produced by scattering the e-beam from a high-power microwave pulse. In recent years, several groups have reported successful x-ray generation via Compton scattering from a *laser pulse*. In 2000, at the Brookhaven National Laboratory Accelerator Test Facility (BNL ATF) collaborators reported [13] generation of 6.5 keV photons by scattering a 10.6 m CO_2 laser from a 60 MeV e-beam. A collaboration at the Lawrence Livermore National Laboratory, at the PLEIADES facility, demonstrated generation of 78 keV x-ray photons [14] using a 57 MeV e-beam and a 820 nm Ti : sapphire laser. An all-optical setup was reported more recently [10], employing a 800 nm Ti : sapphire laser split into two pulses: one used for the acceleration of electrons (5 MeV) and the second, counter-propagating pulse, used for Compton scattering. The emerging photons were measured to be in the range from 0.4 to 2 keV. In addition to Compton scattering based on e-beams produced by photocathode rf-guns, more elaborate methods of laser back-scattering from relativistic mirrors have been recently proposed. Bulanov *et al* [15] proposed a mechanism for coherent back-scattering of a laser from counter-propagating plasma density spikes, acting as flying parabolic relativistic mirrors, created using short and intense laser pulses. Additionally, coherent back-scattering of a laser pulse from dense relativistic electron layers (mirrors), created by laser irradiation of nanometre-thin foils, has been theoretically and numerically analysed [16, 17].

Karagodsky and Schachter, Plasma Phys. Control. Fusion **53** (2011) 014007

Energy

- Layout

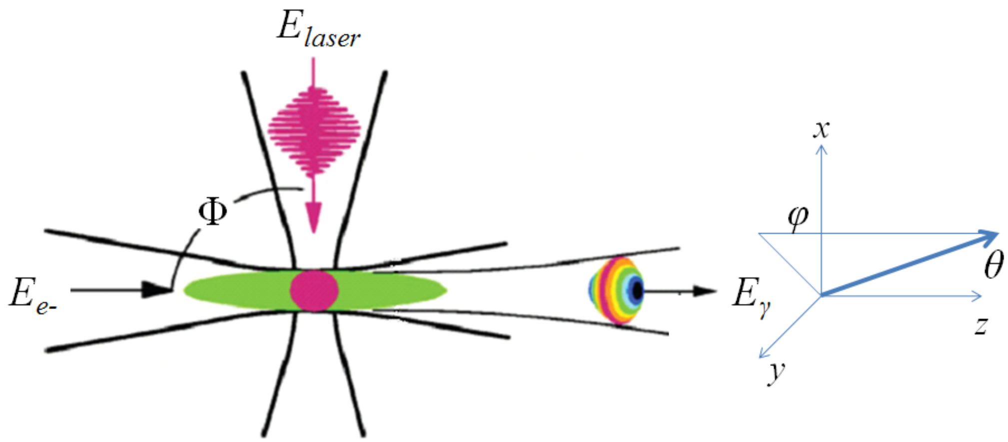

- Energy

$$E_\gamma(\theta,\varphi) = \frac{E_{\text{laser}}(1-\beta\cos\Phi)}{1-\beta\cos\theta + E_{\text{laser}}(1-\cos\Delta\Theta)/E_{e^-}}$$

- Thomson limit

$$E'_{\text{laser}} << mc^2, \qquad E_\gamma(\theta,\phi) \approx E_{\text{laser}} \frac{1-\beta\cos\Phi}{1-\beta\cos\theta}$$

Field Strength Parameter

- Early 1960s: Laser Invented
- Brown and Kibble (1964): Earliest definition of the field strength parameters (normalized vector potential) *K* and/or *a* in the literature that I'm aware of

  $$a = \frac{eE_0\lambda_0}{2\pi mc^2} \quad \text{Compton/Thomson Sources} \qquad K = \frac{eB_0\lambda_0}{2\pi mc} \quad \text{Undulators}$$

  Interpreted frequency shifts that occur at high fields as a "relativistic mass shift".
- Sarachik and Schappert (1970): Power into harmonics at high *K* and/or *a* . Full calculation for CW (monochromatic) laser. Later referenced, corrected, and extended by workers in fusion plasma diagnostics.
- Alferov, Bashmakov, and Bessonov (1974): Undulator/Insertion Device theories developed under the assumption of constant field strength. Numerical codes developed to calculate "real" fields in undulaters.
- Coisson (1979): Simplified undulater theory, which works at low *K* and/or *a,* developed to understand the frequency distribution of "edge" emission, or emission from "short" magnets, i.e., including pulse effects

Spectrum from a "Short" Magnet

Coisson low-field strength undulater spectrum*

$$\frac{dU_\gamma}{d\nu\, d\Omega} = \frac{r_e^2 c}{\pi}\gamma^2\left(1+\gamma^2\theta^2\right)^2 f^2\left|\tilde{B}\left(\nu\left(1+\gamma^2\theta^2\right)/2\gamma^2\right)\right|^2$$

$$f^2 = f_\sigma^2 + f_\pi^2$$

$$f_\sigma = \frac{1}{\left(1+\gamma^2\theta^2\right)^2}\sin\phi$$

$$f_\pi = \frac{1}{\left(1+\gamma^2\theta^2\right)^2}\left(\frac{1-\gamma^2\theta^2}{1+\gamma^2\theta^2}\right)\cos\phi$$

$$r_e^2 \equiv \frac{e^4}{16\pi^2\varepsilon_0^2 m^2 c^4}$$

*R. Coisson, Phys. Rev. A **20**, 524 (1979)

Dipole Radiation

$$\vec{B} = \frac{\mu_0 e\ddot{d}\left(t - r/c\right)}{4\pi c r}\sin\Theta\hat{\Phi}$$

$$\vec{E} = \frac{\mu_0 e\ddot{d}\left(t - r/c\right)}{4\pi r}\sin\Theta\hat{\Theta}$$

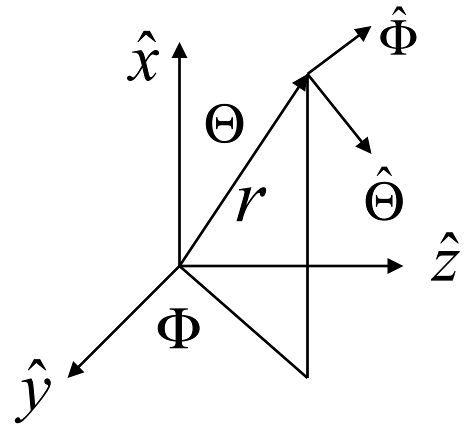

$$I = \frac{\vec{E}\times\vec{B}}{\mu_0} = \frac{\mu_0}{16\pi^2}\frac{e^2\ddot{d}^2\left(t - r/c\right)}{c r^2}\sin^2\Theta\hat{r}$$

$$\frac{dI}{d\Omega} = \frac{1}{16\pi^2\varepsilon_0}\frac{e^2\ddot{d}^2\left(t - r/c\right)}{c^3}\sin^2\Theta$$

Polarized in the plane containing $\hat{r} = \vec{n}$ and $\hat{x}$

Dipole Radiation

Define the Fourier Transform

$$\tilde{d}(\omega)=\int d(t)e^{-i\omega t}dt \qquad d(t)=\frac{1}{2\pi}\int \tilde{d}(\omega)e^{i\omega t}d\omega$$

With these conventions Parseval's Theorem is

$$\int d^2(t)dt=\frac{1}{2\pi}\int \left|\tilde{d}\right|^2(\omega)d\omega$$

$$\frac{dU_\gamma}{d\Omega}=\frac{e^2}{16\pi^2\varepsilon_0 c^3}\int \ddot{d}^2(t-r/c)\,dt=\frac{e^2}{32\pi^3\varepsilon_0 c^3}\int \omega^4\left|\tilde{d}\right|^2(\omega)\,d\omega$$

$$\frac{dU_\gamma}{d\omega d\Omega}=\frac{1}{32\pi^3\varepsilon_0}\frac{e^2\omega^4\left|\tilde{d}(\omega)\right|^2}{c^3}\sin^2\Theta$$

Blue Sky!

This equation does not follow the typical (see Jackson) convention that combines both positive and negative frequencies together in a single positive frequency integral. The reason is that we would like to apply Parseval's Theorem easily. By symmetry, the difference is a factor of two.

Comments/Sum Rule

- There is no radiation parallel or anti-parallel to the *x*-axis for *x*-dipole motion (gives the 0.5 in Compton's curve)
- In the forward direction $\theta' \to 0$, the radiation polarization is parallel to the *x*-axis for an *x*-dipole motion

$$\frac{dU'_{\gamma,\sigma}}{d\omega'} = \frac{1}{32\pi^3\varepsilon_0}\frac{e^2\omega'^4}{c^3}\left(\left|\tilde{d}'_x(\omega')\right|^2 + \left|\tilde{d}'_y(\omega')\right|^2\right)2\pi$$

$$\frac{dU'_{\gamma,\pi}}{d\omega'} = \frac{1}{32\pi^3\varepsilon_0}\frac{e^2\omega'^4}{c^3}\left[\left(\left|\tilde{d}'_x(\omega')\right|^2 + \left|\tilde{d}'_y(\omega')\right|^2\right)\frac{2\pi}{3} + \left|\tilde{d}'_z(\omega')\right|^2\frac{8\pi}{3}\right]$$

$$\frac{dU'_{\gamma}}{d\omega'} = \frac{1}{32\pi^3\varepsilon_0}\frac{e^2\omega'^4\left|\tilde{\vec{d}}'(\omega')\right|^2}{c^3}\frac{8\pi}{3}$$

Generalized Larmor (in frequency space)

Sum Rule

Total energy sum rule

$$U'_{tot} = \int_{-\infty}^{\infty} \frac{1}{12\pi^2\varepsilon_0} \frac{e^2\omega'^4 \left|\tilde{\vec{d}}'(\omega')\right|^2}{c^3} d\omega'$$

Parseval's Theorem again gives "standard" Larmor formula

$$P' = \frac{dU'_{tot}}{dt'} = \frac{1}{6\pi\varepsilon_0} \frac{e^2\ddot{\vec{d}}'^2(t')}{c^3} = \frac{1}{6\pi\varepsilon_0} \frac{e^2\vec{a}'^2(t')}{c^3}$$

Weak Field Undulator Spectrum

$$\tilde{\vec{d}}'(\omega') = \tilde{d}'(\omega')\hat{x} = -\frac{ec}{mc^2}\frac{\tilde{B}(\omega'/c\beta_z\gamma)}{\omega'^2}\hat{x} \qquad \tilde{B}(k) = \int B(z)e^{-ikz}dz$$

$$\frac{dU_{\gamma,\sigma}}{d\omega d\Omega} = \frac{1}{32\pi^3\varepsilon_0}\frac{e^4}{m^2c^5}\frac{\left|\tilde{B}\left(\omega(1-\beta_z\cos\theta)/c\beta_z\right)\right|^2}{\gamma^2(1-\beta_z\cos\theta)^2}\sin^2\phi$$

$$\frac{dU_{\gamma,\pi}}{d\omega d\Omega} = \frac{1}{32\pi^3\varepsilon_0}\frac{e^4}{m^2c^5}\frac{\left|\tilde{B}\left(\omega(1-\beta_z\cos\theta)/c\beta_z\right)\right|^2}{\gamma^2(1-\beta_z\cos\theta)^2}\left(\frac{\cos\theta-\beta_z}{1-\beta_z\cos\theta}\right)^2\cos^2\phi$$

$$\lambda = \frac{\lambda_0}{2\gamma^2} \qquad (1-\beta_z\cos\theta)(1+\beta_z) \approx \frac{1}{\gamma^2}+\theta^2+\ldots \approx \frac{1+\gamma^2\theta^2}{\gamma^2}$$

Generalizes Coisson to arbitrary observation angles

Weak Field Thomson Backscatter

With $\Phi = \pi$ and $a << 1$ the result is identical to the weak field undulator result with the replacement of the magnetic field Fourier transform by the electric field Fourier transform

	Undulator	Thomson Backscatter
Driving Field	$\tilde{B}_y\left(\omega\left(1-\beta_z\cos\theta\right)/c\beta_z\right)$	$\tilde{E}_x\left(\omega\left(1-\beta_z\cos\theta\right)/\left(c\left(1+\beta_z\right)\right)\right)$
Forward Frequency	$\lambda \approx \dfrac{\lambda_0}{2\gamma^2}$	$\lambda \approx \dfrac{\lambda_0}{4\gamma^2}$
	Lorentz contract + Doppler	Double Doppler

Handy Formulas

$$\frac{d^2U_\gamma}{d\omega d\Omega} = \frac{r_e^2\varepsilon_0}{2\pi c}\left|\tilde{E}\left[\frac{\omega\left(1-\beta\cos\theta\right)}{c\left(1+\beta\right)}\right]\right|^2 \times$$

$$\frac{\sin^2\phi\left(1-\beta\cos\theta\right)^2+\cos^2\phi\left(\cos\theta-\beta\right)^2}{\gamma^2\left(1-\beta\cos\theta\right)^{2\cdot 2}}$$

$$U_\gamma = \gamma^2\left(1+\beta\right)\frac{N_e\sigma_T}{\left(\sigma_e^2+\sigma_{laser}^2\right)}$$

$$N_\gamma = \sigma_T\frac{N_eN_{laser}}{2\pi\left(\sigma_e^2+\sigma_{laser}^2\right)}$$

$$N_{\gamma,\mathrm{per}\ e} = \frac{2\pi\alpha N_\lambda a^2}{3}$$

Number Distribution of Photons

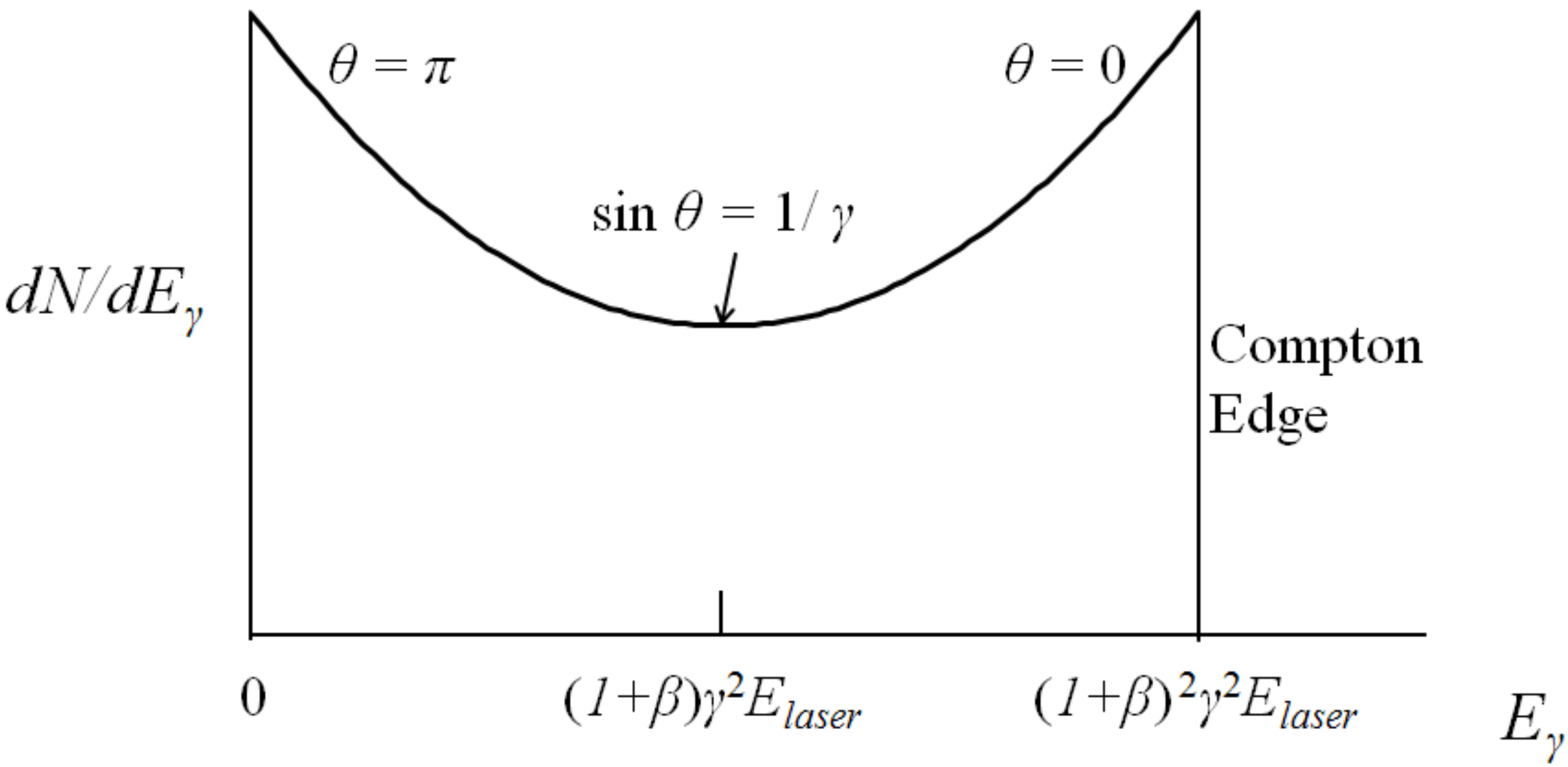

Flux

- Percentage in 0.1% bandwidth ($\theta = 0$)

$$N_{0.1\%} = 1.5 \times 10^{-3} N_\gamma$$

- Flux into 0.1% bandwidth

$$\mathcal{F} = 1.5 \times 10^{-3} \dot{N}_\gamma$$

- Flux for high rep rate source

$$\mathcal{F} = 1.5 \times 10^{-3} f N_\gamma$$

Energy Spread

Sources of Energy Spread in the Scattered Pulse

Source Term	Estimate	Comment
Beam energy spread	$2\sigma_{E_{e-}} / E_{e-}$	From FEL resonance
Laser pulse width	σ_{ω} / ω	Doppler Freq Indepedent
Finite θ acceptance (full width)	$\gamma^2 \Delta\theta^2$	θ = 0 for experiments
Finite beam emittance	$2\gamma^2 \varepsilon / \beta_{e-}$	Beta-function

Spectral Brilliance

- In general

$$\mathcal{B} = \frac{\mathcal{F}}{4\pi^2 \sigma_x \sigma_{x'} \sigma_y \sigma_{y'}}$$

$$\approx \frac{\mathcal{F}}{4\pi^2 \sqrt{\beta_x \varepsilon_x} \sqrt{\varepsilon_x / \beta_x + \lambda / 2L} \sqrt{\beta_y \varepsilon_y} \sqrt{\varepsilon_y / \beta_y + \lambda / 2L}}$$

- For Compton scattering from a low energy beam

$$\mathcal{B} = \frac{\mathcal{F}}{4\pi^2 \varepsilon_x \varepsilon_y}$$

Compton Polarimetry

- At high photon energy (in beam frame), scattering rate couples to the polarization variables

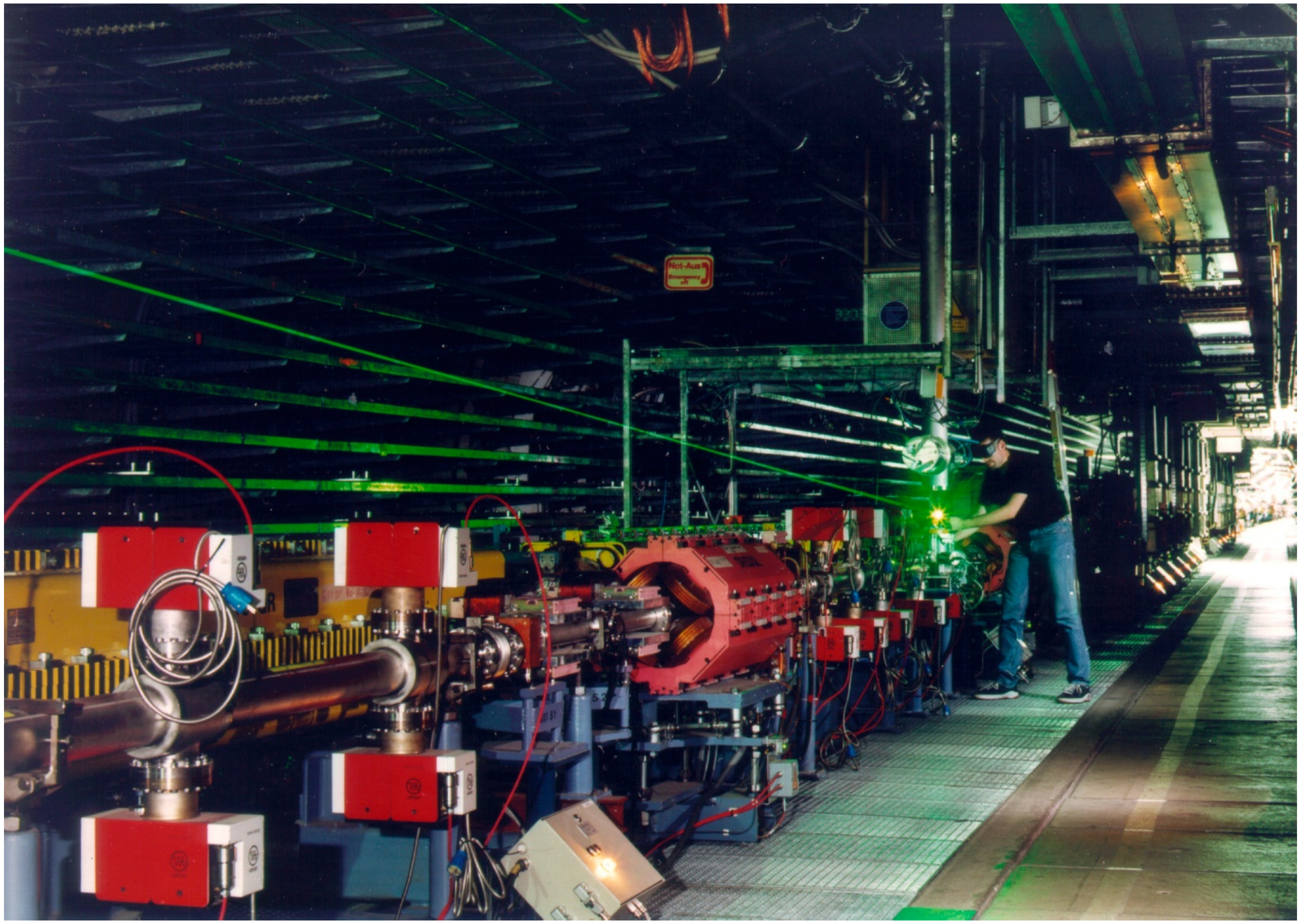

High *a/K*

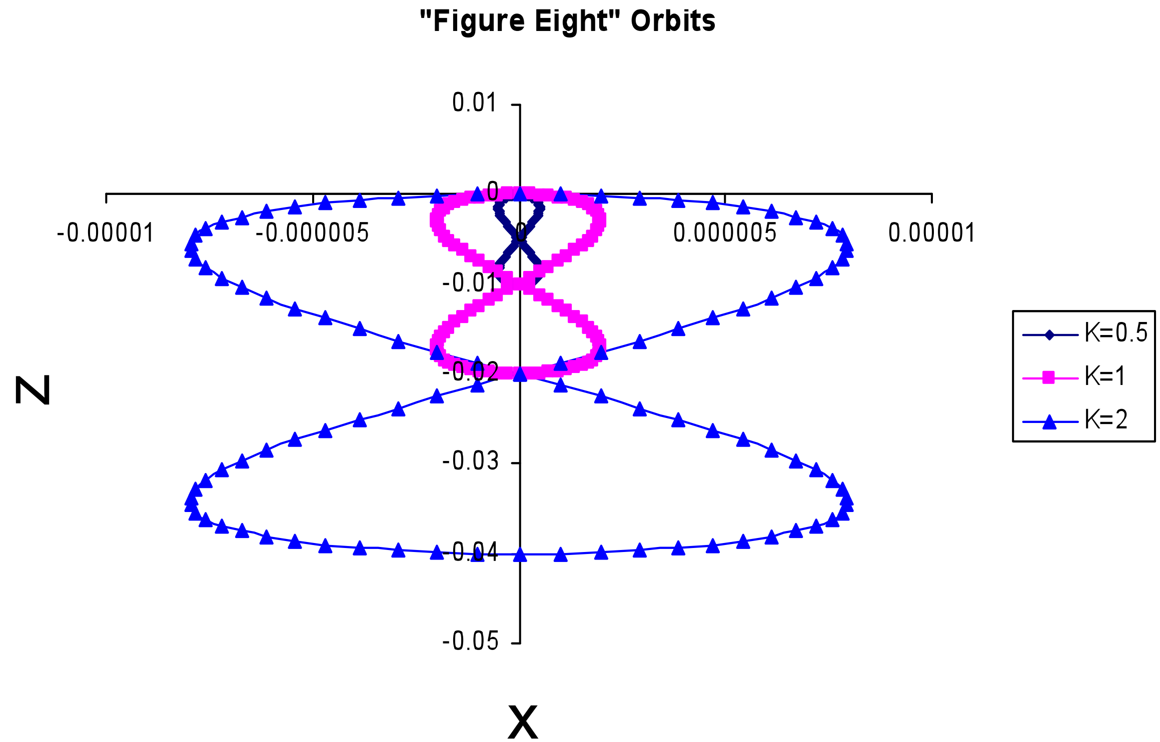

γ = 100, distances are normalized by $\lambda_0 / 2\pi$

Energy Distribution

$$\frac{dU_{\gamma,\sigma}}{d\omega d\Omega}=\frac{e^2\omega^2}{32\pi^3\varepsilon_0 c^3}\left|\begin{matrix} D_t(\omega;\theta,\varphi)\sin\varphi \\ -\dfrac{\sin\Phi}{\gamma(1-\beta\cos\Phi)}D_p(\omega;\theta,\varphi)\cos\varphi \end{matrix}\right|^2$$

$$\frac{dU_{\gamma,\pi}}{d\omega d\Omega}=\frac{e^2\omega^2}{32\pi^3\varepsilon_0 c^3}\left|\begin{matrix} D_t(\omega;\theta,\varphi)\dfrac{\cos\theta-\beta}{1-\beta\cos\theta}\cos\varphi \\ +\dfrac{\sin\Phi}{\gamma(1-\beta\cos\Phi)}D_p(\omega;\theta,\varphi)\dfrac{\cos\theta-\beta}{1-\beta\cos\theta}\sin\varphi \\ +\dfrac{\beta-\cos\Phi}{1-\beta\cos\Phi}D_p(\omega;\theta,\varphi)\dfrac{\sin\theta}{\gamma(1-\beta\cos\theta)} \end{matrix}\right|^2$$

Effective Dipole Motions

$$D_t(\omega;\theta,\varphi)=\frac{1}{\gamma(1-\beta\cos\Phi)}\int\frac{eA(\xi)}{mc}e^{i\phi(\omega,\xi;\theta,\varphi)}d\xi$$

$$D_p(\omega;\theta,\varphi)=\frac{1}{\gamma(1-\beta\cos\Phi)}\int\frac{e^2A^2(\xi)}{2m^2c^2}e^{i\phi(\omega,\xi;\theta,\varphi)}d\xi$$

And the (Lorentz invariant!) phase is

$$\varphi(\omega,\xi;\theta,\phi)=\frac{\omega}{c}\left(\begin{array}{l}\xi\dfrac{(1-\beta\cos\theta)}{(1-\beta\cos\Phi)}-\dfrac{\sin\theta\cos\phi}{\gamma(1-\beta\cos\Phi)}\displaystyle\int_{-\infty}^{\xi}\frac{eA(\xi')}{mc}d\xi'\\+\dfrac{1-\sin\theta\sin\phi\sin\Phi-\cos\theta\cos\Phi}{\gamma^2(1-\beta\cos\Phi)^2}\displaystyle\int_{-\infty}^{\xi}\frac{e^2A^2(\xi')}{2m^2c^2}d\xi'\end{array}\right)$$

High Field Thomson Backscatter

For a flat incident laser pulse the main results are very similar to those from undulaters with the following correspondences

	Undulater	Thomson Backscatter
Field Strength	K	a
Forward Frequency	$\lambda \approx \frac{\lambda_0}{2\gamma^2}\left(1+\frac{K^2}{2}\right)$	$\lambda \approx \frac{\lambda_0}{4\gamma^2}\left(1+\frac{a^2}{2}\right)$
Transverse Pattern	$\beta^*_z + \cos\theta'$	$1+\cos\theta'$

NB, be careful with the radiation pattern, it is the same at small angles, but quite a bit different at large angles

Modifications at High *a*

- Resonance frequency in forward direction red-shifts

$$E_{\gamma,n} = n\frac{4\gamma^2 E_{laser}}{1+a^2/2}$$

- Flux into the *n*th harmonic (*n* odd)

$$F_n(a) = \frac{n^2 a^2}{\left(1+a^2/2\right)^2}\left\{ J_{(n-1)/2}\left[\frac{na^2}{4\left(1+a^2/2\right)}\right] - J_{(n+1)/2}\left[\frac{na^2}{4\left(1+a^2/2\right)}\right]\right\}$$

- Non-flat illumination pulses give ponderomotive broadening

Flat Illumination Pulse

20-period
equivalent undulater: $A_x(\xi) = A_0 \cos(2\pi\xi/\lambda_0)[\Theta(\xi) - \Theta(\xi - 20\lambda_0)]$

$$\omega_0 \equiv (1+\beta_z)^2 \gamma^2 2\pi c/\lambda_0 \approx 4\gamma^2 2\pi c/\lambda_0, \quad a = eA_0/mc$$

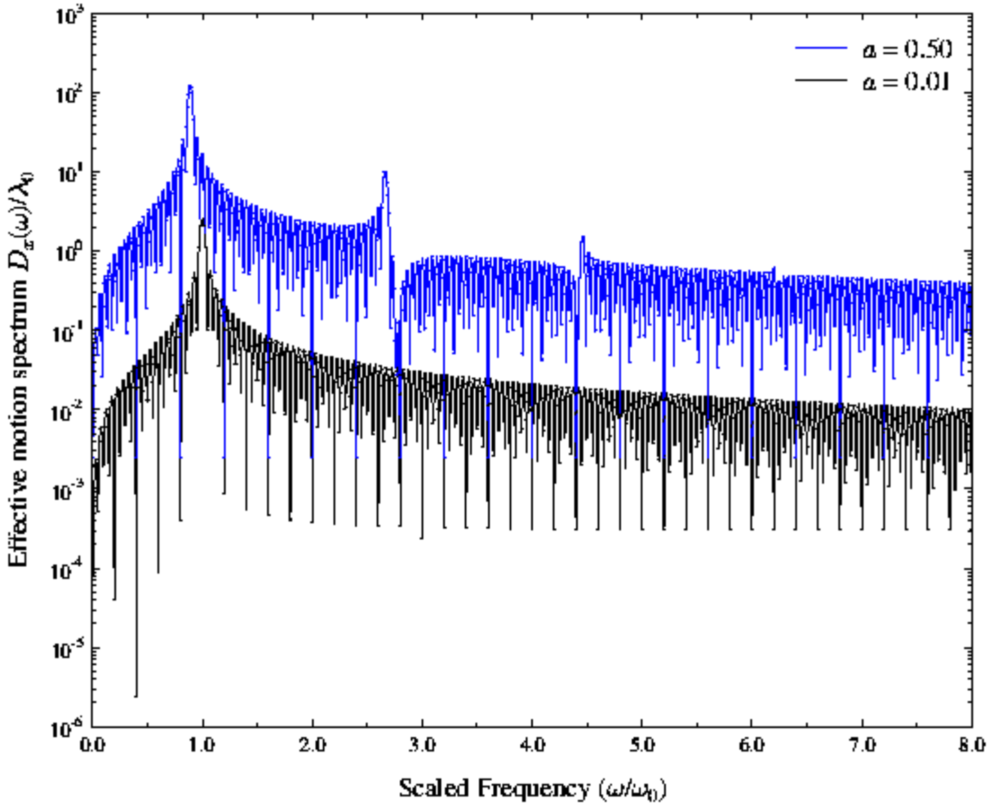

$$1/\left(1+a^2/2\right)$$

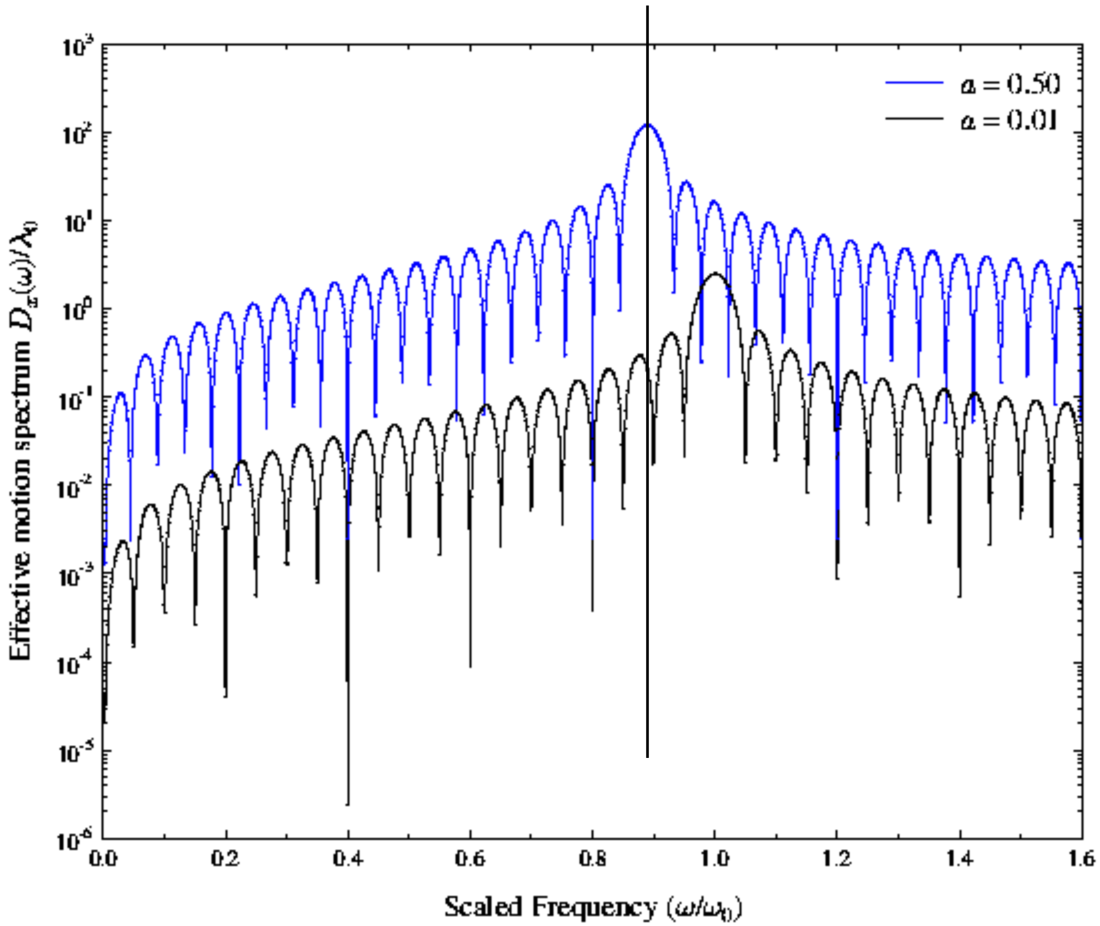

Spectral Broadening: Gaussian Pulse

$$A_x(\xi) = A_{peak}\exp\left(-z^2/2(8.156\lambda_0)^2\right)\cos(2\pi\xi/\lambda_0) \qquad a_{peak} = eA_{peak}/mc$$

A_{peak} and λ_0 chosen for same intensity and same *rms* pulse length as previous slide

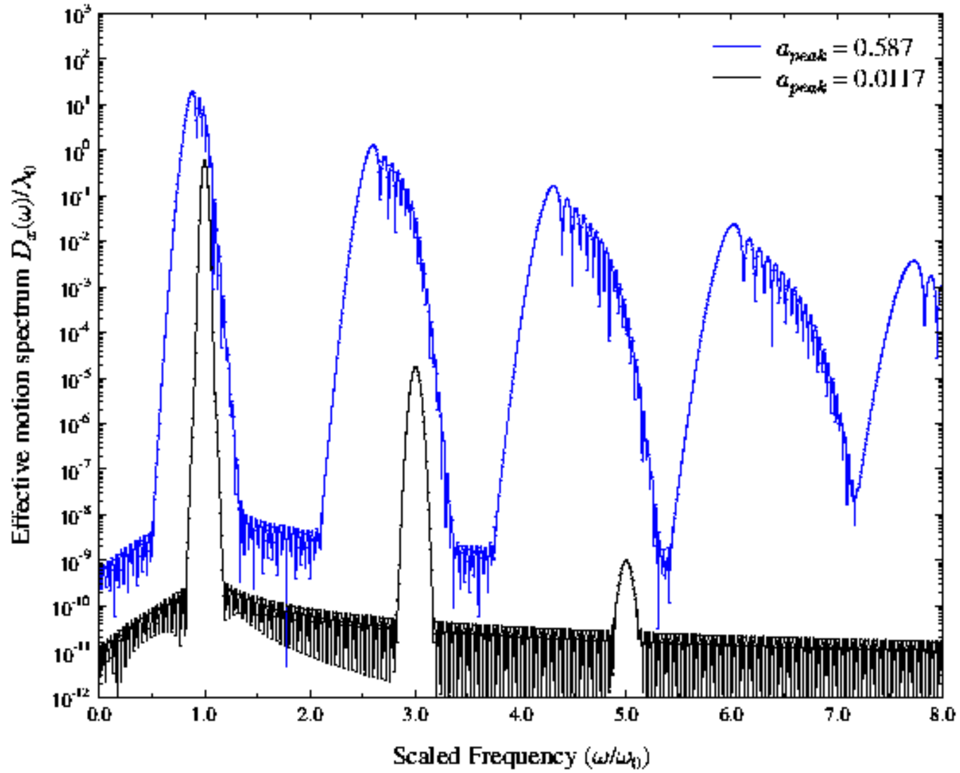

G. A. Krafft, Phys. Rev. Lett., **92**, 204802 (2004)

Source Illumination Method

- Direct illumination by laser
  - Earliest method
  - Deployed on storage rings
- Optical cavities
  - Self-excited
  - Externally excited
  - Deployed on rings, linacs, and energy recovered linacs
- High power single pulses
  - Deployed on linacs

Early Gamma Ray Sources

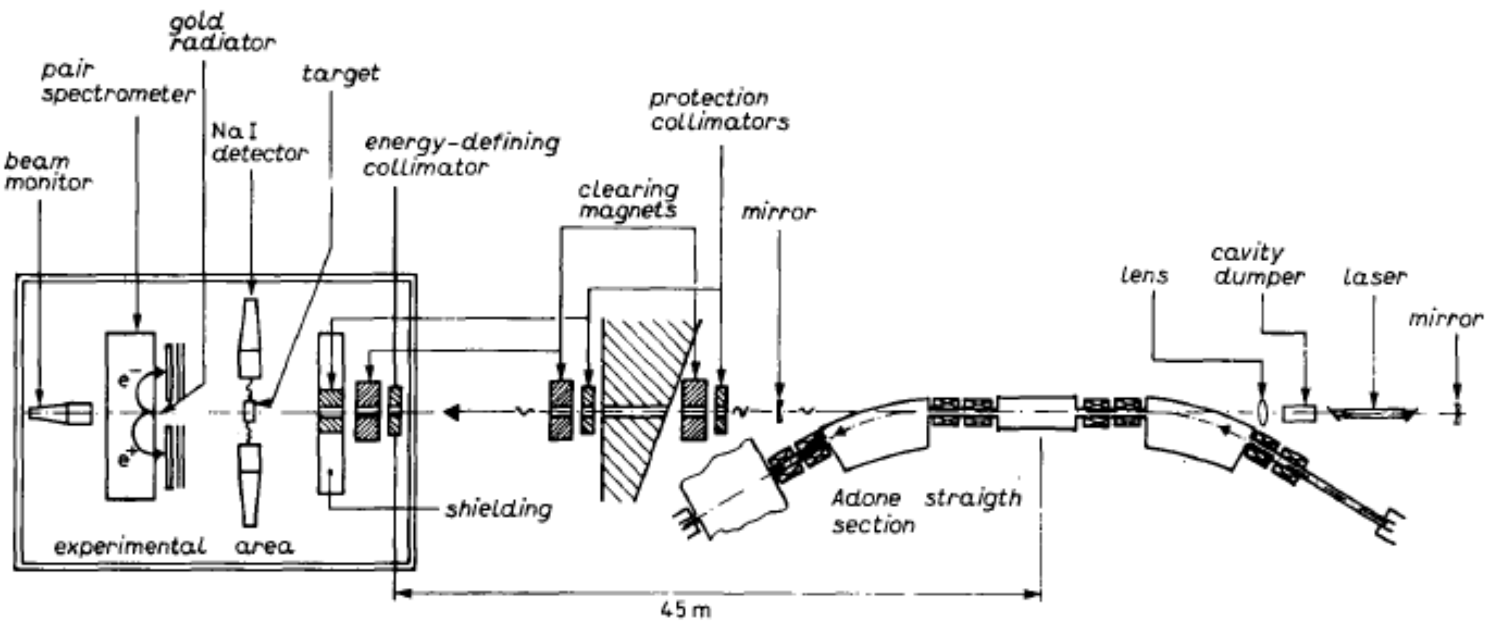

Fig. 1. – Overall view of the experimental set-up.

Compton Edge
78 MeV

Federici, *et al.*
Nouvo. Cim. B 59, 247 (1980)

LEGS

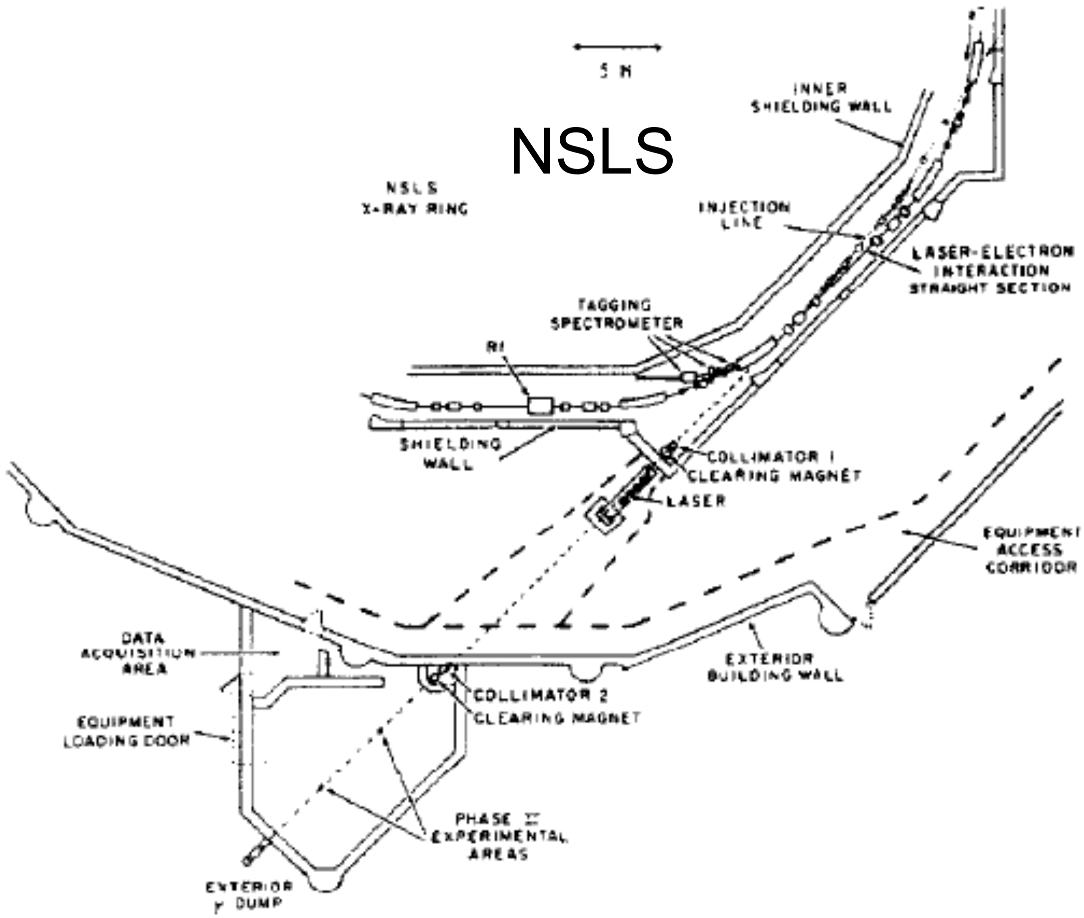

Fig. 4 A plan of the LEGS facility at BNL.

Compton Edge
270 MeV

Sandorfi, *et al.*
PAC83, 3083 (1983)

Electrotechnical Laboratory (Japan)

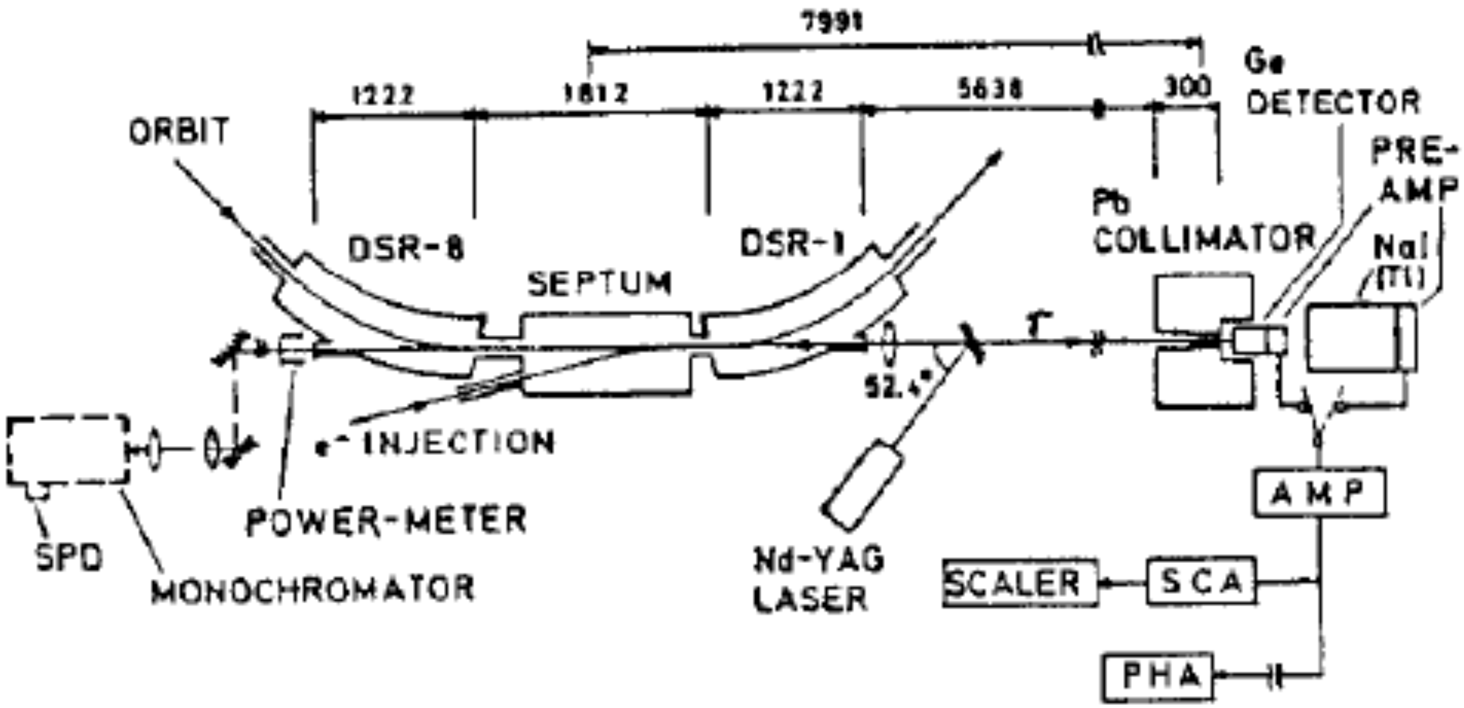

Fig. 2. Experimental arrangement.

Compton Edge 6.5 MeV

Yamazaki, *et al.*
PAC85, 3406 (1985)

Optical Cavities

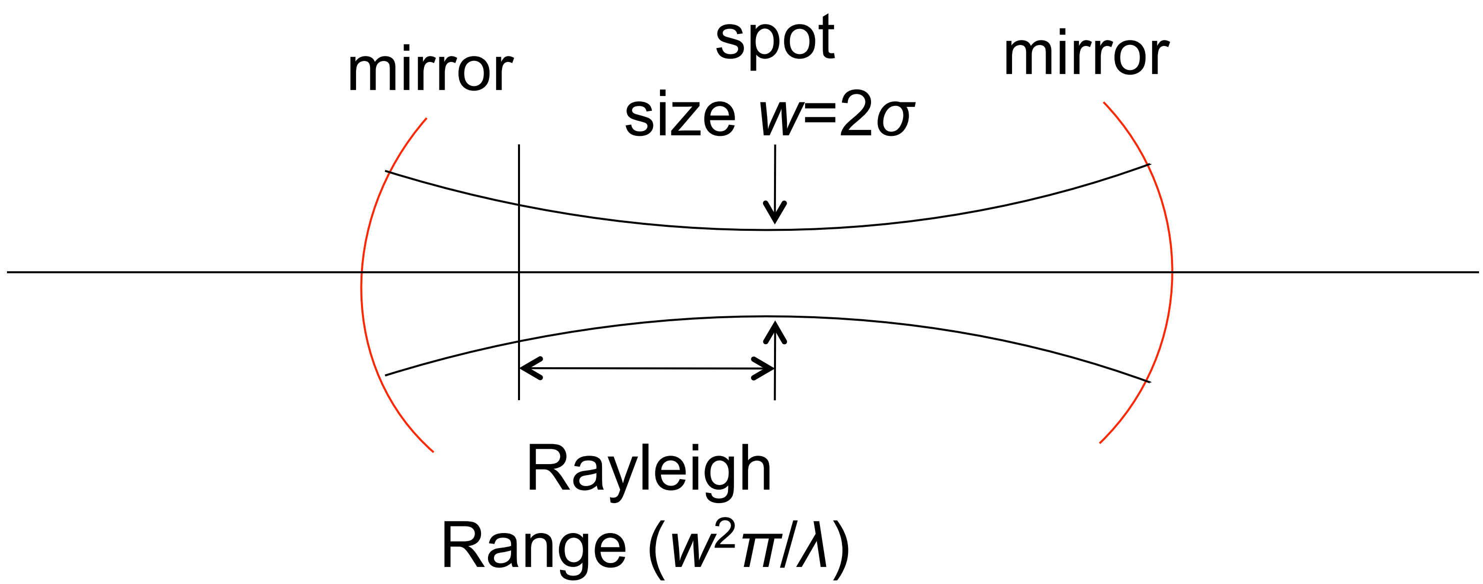

Quantity	Dimensions
Wavelength	200 nm-10 microns
Circulating Power	0.1-200 kW
Spot Size	50-500 microns
Rayleigh Range	40 cm-5 m

Self Excited

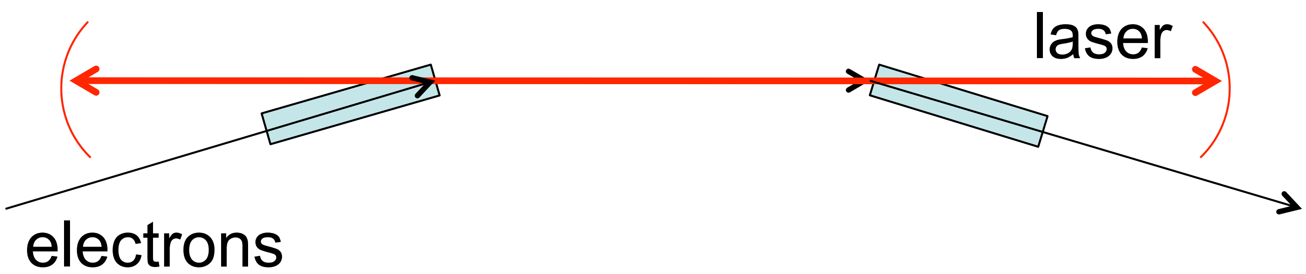

Location	Wavelength	Circulating Power	Spot Size	Rayleigh Range
Orsay	5 microns	100 W	mm	0.7 m
UVSOR	466 nm	20 W	250 microns	0.4 m
Duke Univ.	545 nm	1.6 kW	930 microns	5 m
Super-ACO	300 nm	190 W	440 microns	2 m
Jefferson Lab FEL	1 micron	100 kW	150 microns	1 m

Externally Excited

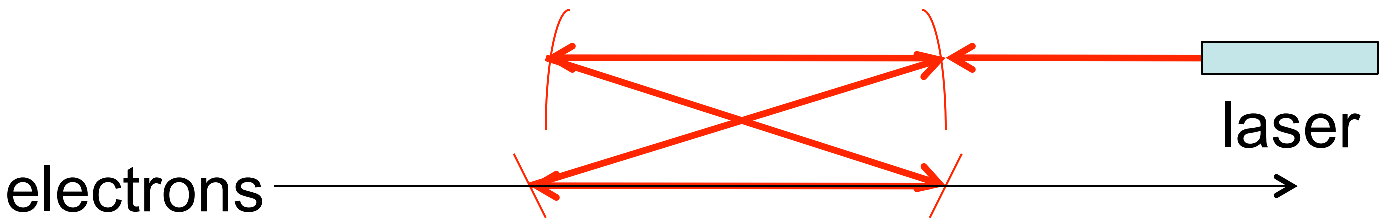

Location	Wavelength	Input Power	Circulating Power	Spot Size (rms)
Jefferson Lab Polarimeter	1064 nm	0.3 W	1.5 kW	120 microns
TERAS	1064 nm	0.5 W	7.5 W	900 microns
Lyncean	1064 nm	7 W	25 kW	60 microns
HERA Polarimeter	1064 nm	0.7 W	2 kW	200 microns
LAL	532 nm	1.0 W	10 kW	40 microns

Modern Ring Based Systems

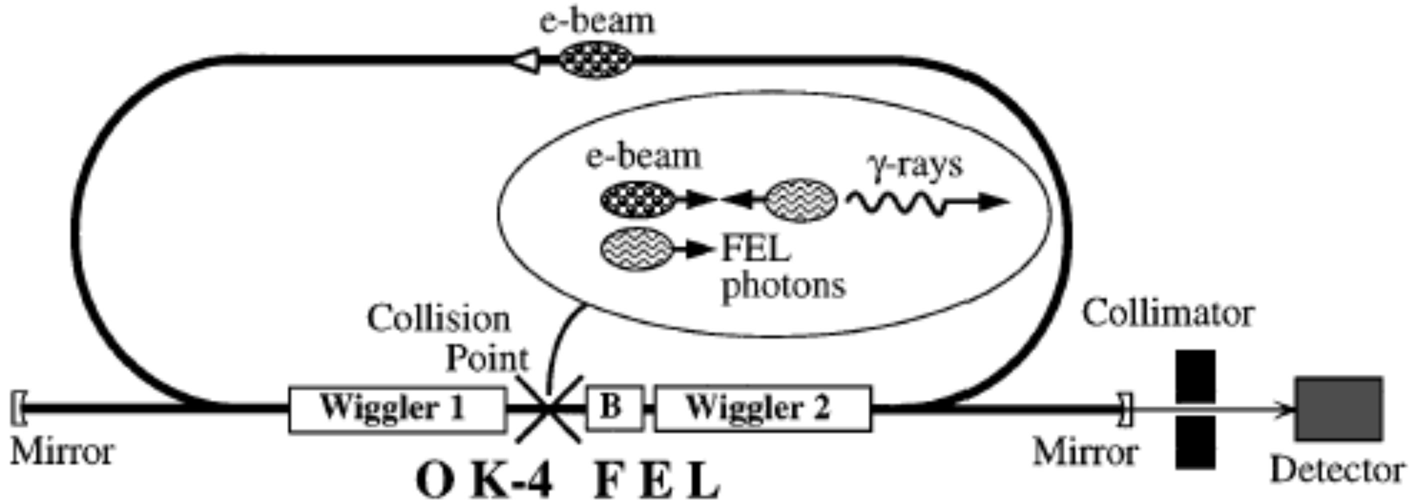

FIG. 1. Schematic of the OK-4/Duke storage ring FEL and γ-ray source. Two electron bunches spatially separated by one-half the circumference of the ring participate both in lasing and γ-ray production via Compton scattering of intracavity photons. A collimator installed downstream selects a narrow cone of quasimonoenergetic γ rays.

Litvinenko, *et al., Phys. Rev. Lett.*, **78**, 4569 (1997)

Duke HIGS Facility

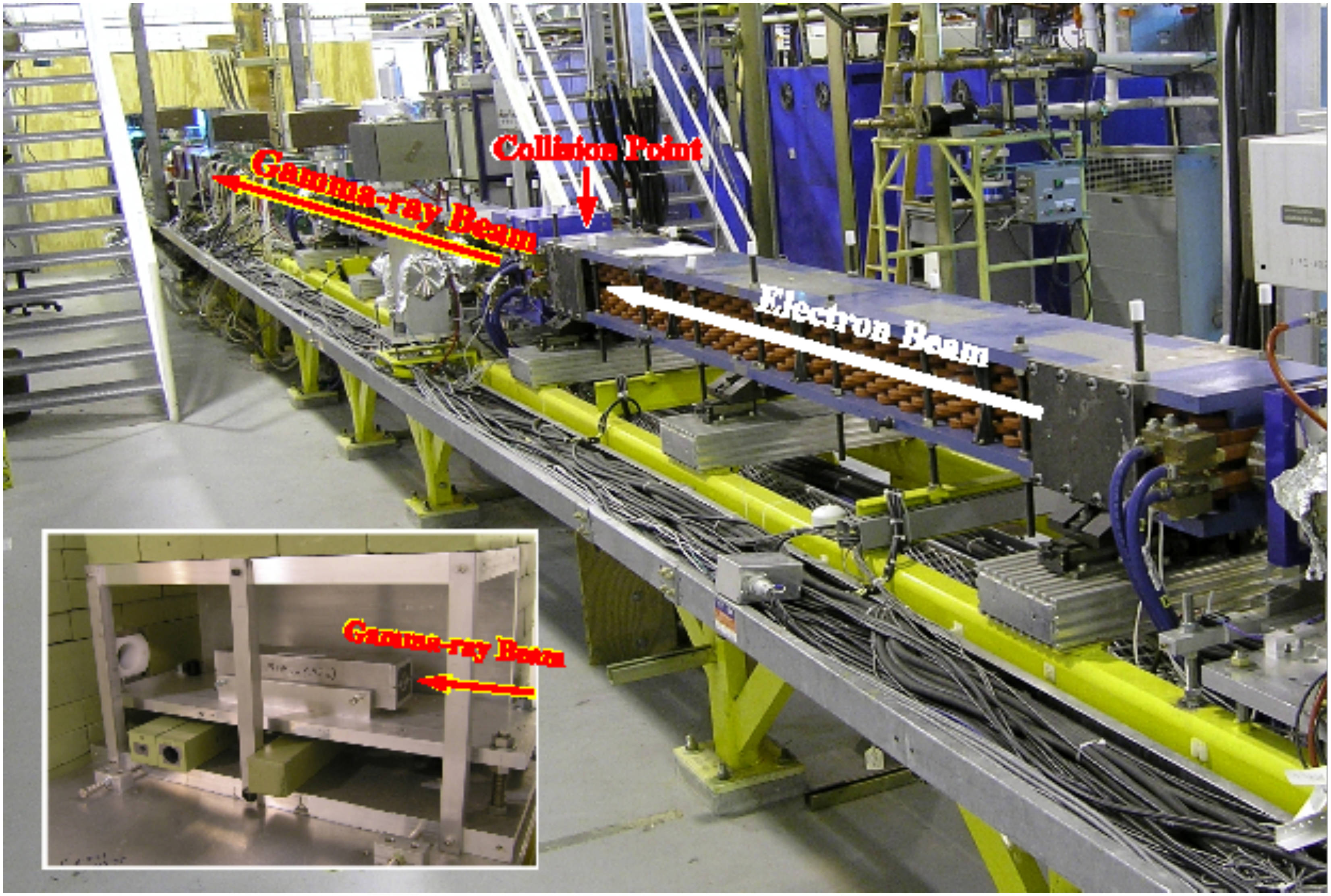

Some Modern Parameters

Parmeter	Value	Unit
Photon Energy	100	MeV
Production Rate	10^{10}	photons/sec@9 MeV
Laser Wavelength	545	nm
Circulating Power	1.6	kW
Polarization	100%	

Topoff allows larger circulating power now!

H. R. Weller, *et al., Prog. Part. Nucl. Phys.*, **62**, 4569 (2009)

Lyncean Compact X-ray Source

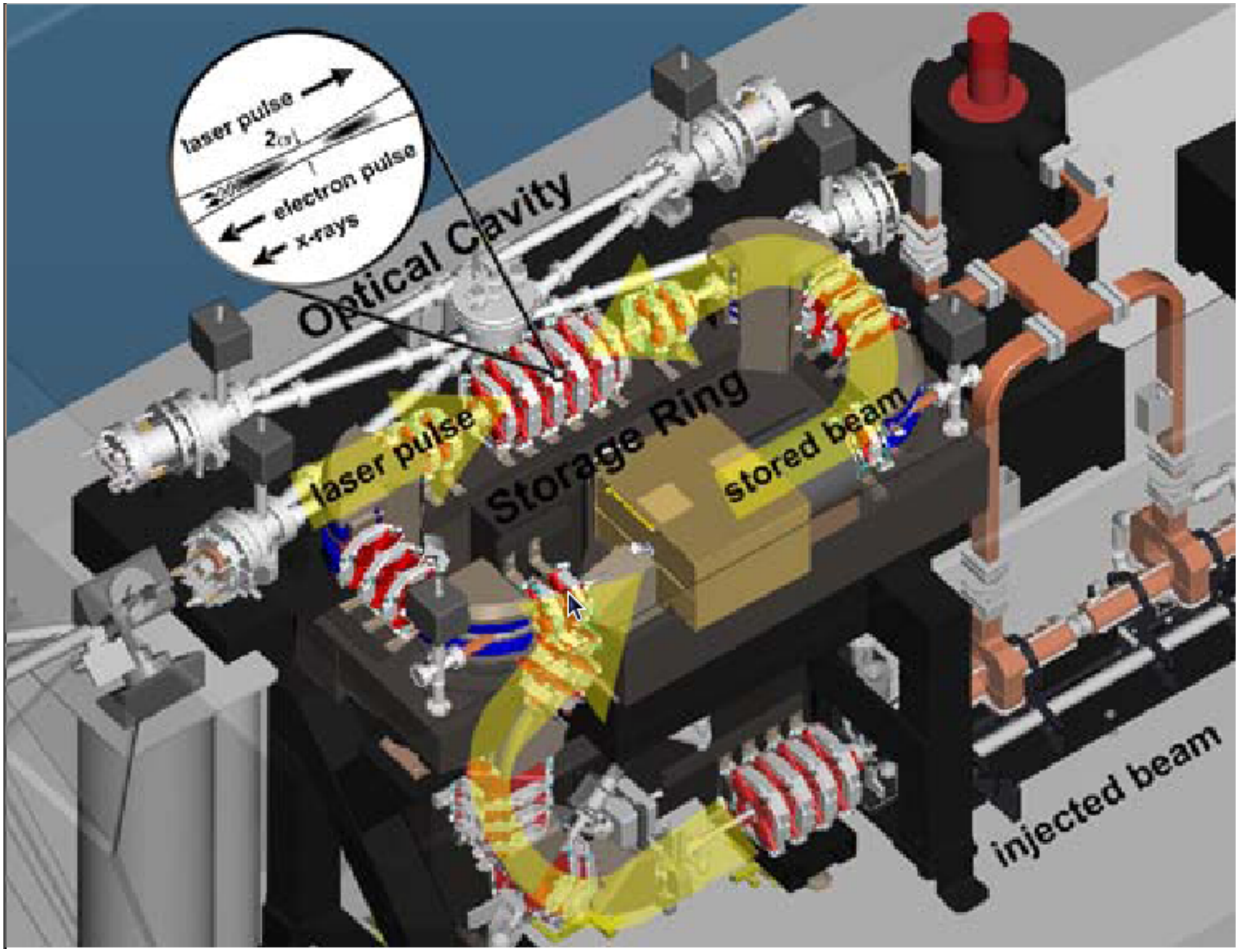

Lyncean Source Performance

Parmeter	Value	Unit
Photon Energy	10-20	keV
Production Rate	10^{11}	photons/sec
Laser Wavelength	1064	nm
Circulating Power	25	kW
Polarization	100%	
Ultimate Brilliance	5×10^{11}	p/(sec mm^{2}mrad^{2}0.1%)

The Jefferson Lab IR FEL

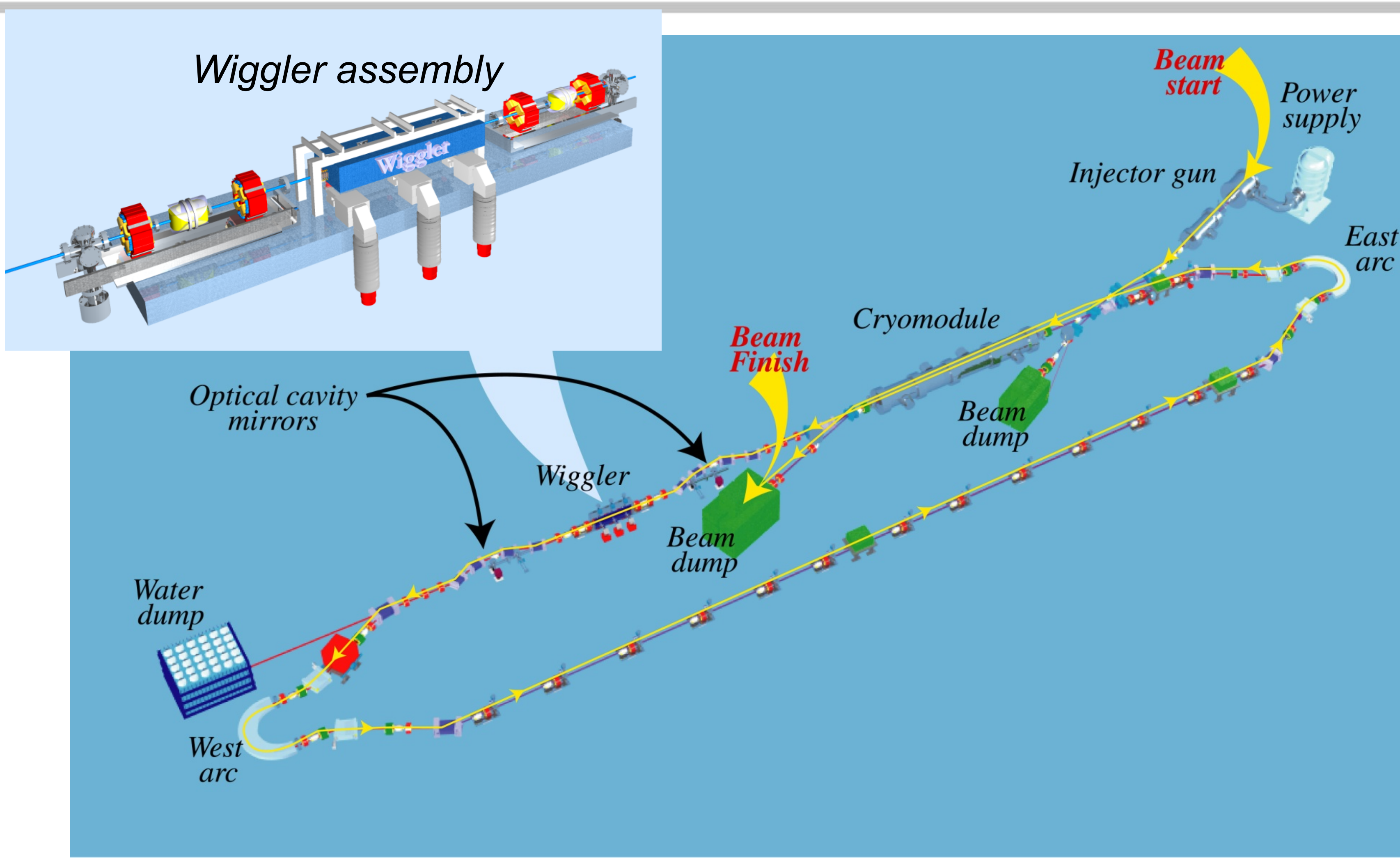

Neil, G. R., *et. al, Physical Review Letters,* **84,** 622 (2000)

FEL Accelerator Parameters

Parameter	Designed	Measured
Kinetic Energy	48 MeV	48.0 MeV
Average current	5 mA	4.8 mA
Bunch charge	60 pC	Up to 135 pC
Bunch length (rms)	<1 ps	0.4±0.1 ps
Peak current	22 A	Up to 60 A
Trans. Emittance (rms)	<8.7 mm-mr	7.5±1.5 mm-mr
Long. Emittance (rms)	33 keV-deg	26±7 keV-deg
Pulse repetition frequency (PRF)	18.7 MHz, x2	18.7 MHz, x0.25, x0.5, x2, and x4

Thomson Source Scattering Geometry

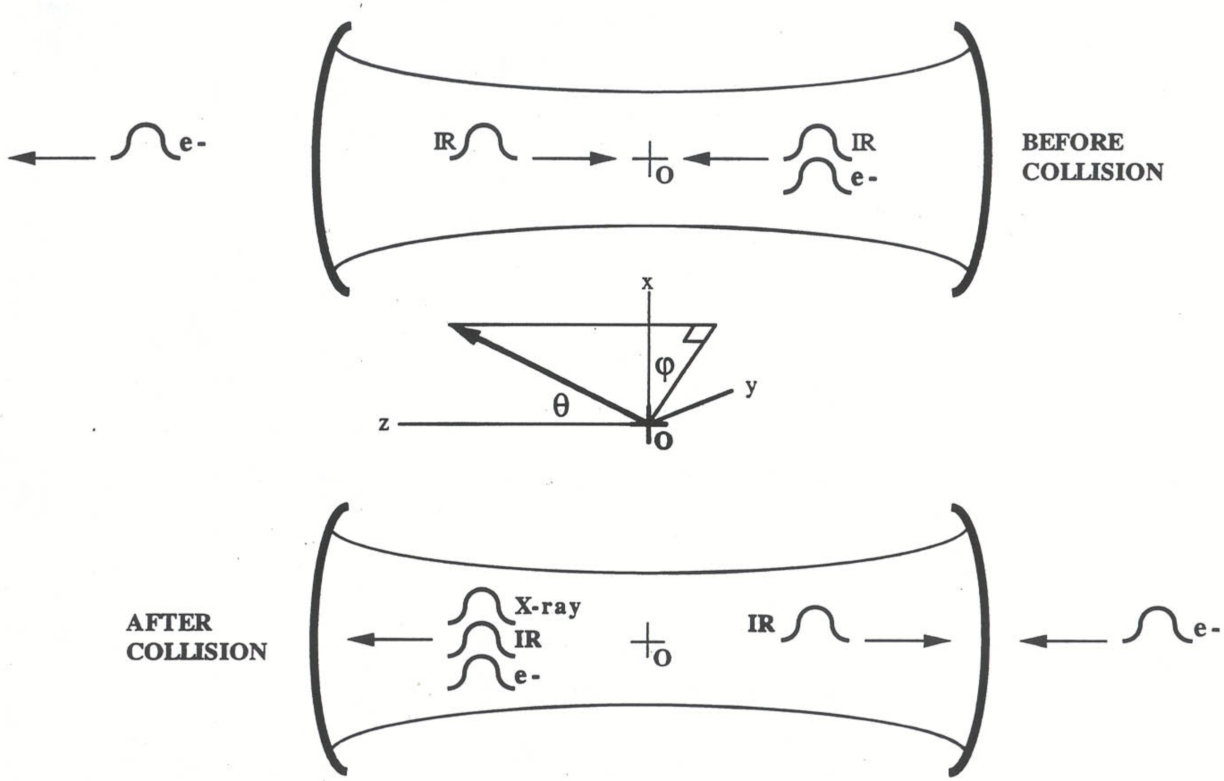

SCATTERING GEOMETRY

60 sec FEL Short-pulse X-ray Spectrum

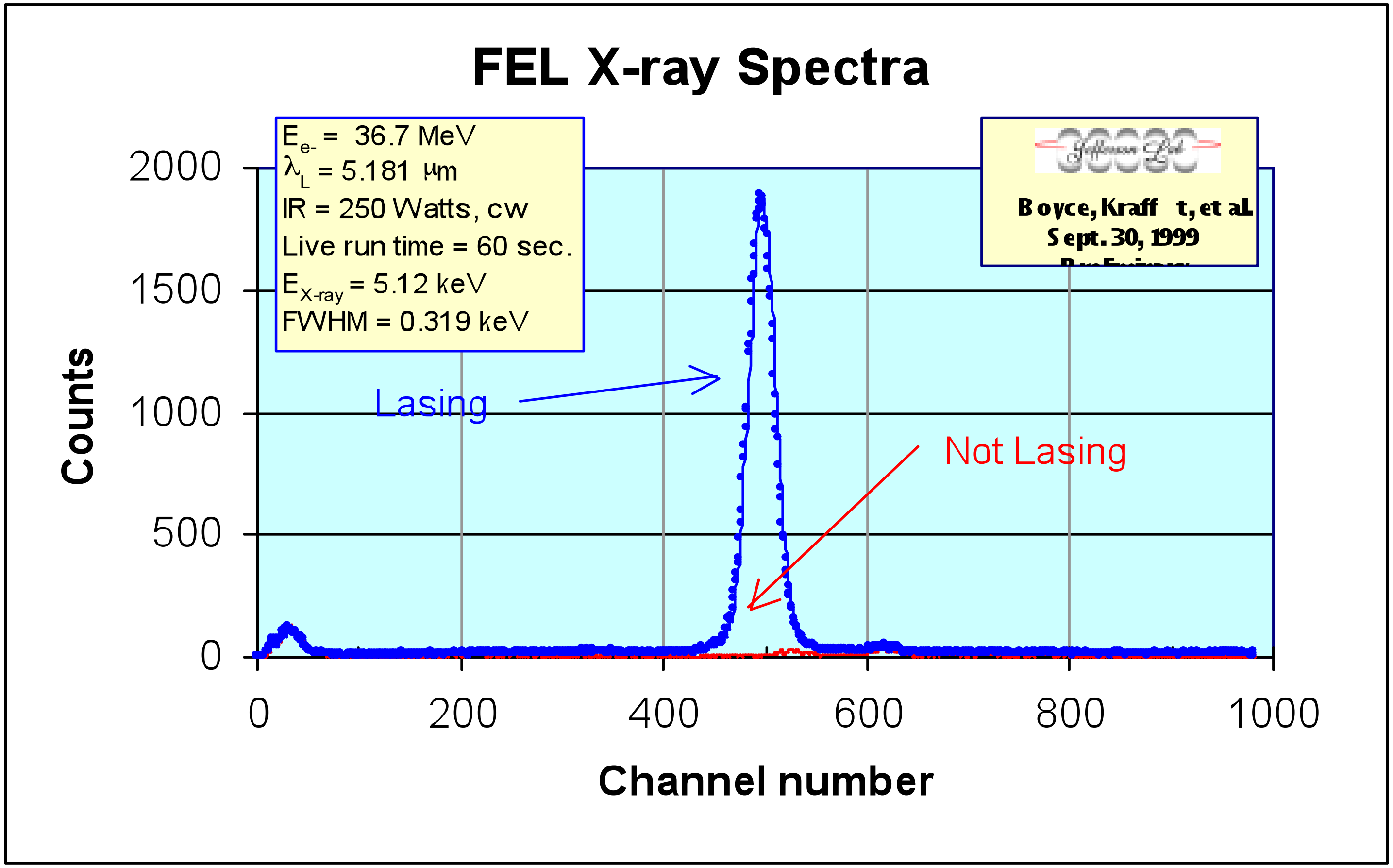

Boyce, *et al.*, 17th Int. Conf. Appl. Accel., 325 (2002)

Linac-based Sources aka Blast Away

- Take the biggest laser you can get and focus to smallest spot you can
- Single shots at low repetition rate
- High peak brilliance (but not at FEL levels)

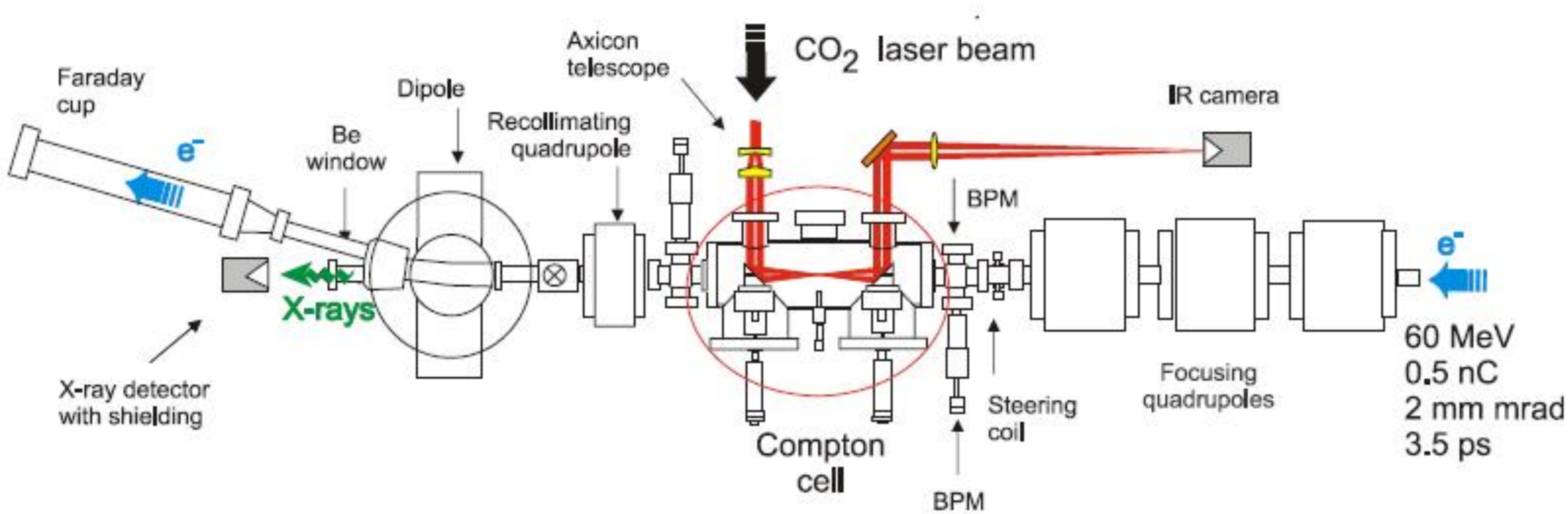

Pogorelsky, *et al., Phys. Rev. ST-AB*, **3**, 090702 (2000)
F. Albert, *et al., Phys. Rev. ST-AB*, **13**, 070704 (2010),
Daresbury ALICE Group

LLNL

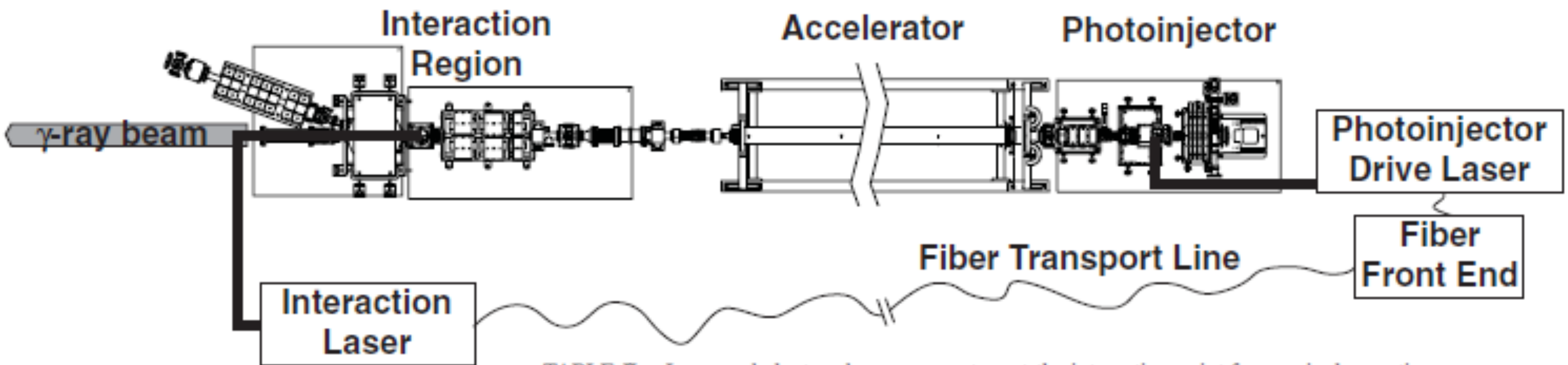

TABLE II. Laser and electron beam parameters at the interaction point for nominal operation.

Laser	
Repetition rate	10 Hz
Wavelength	532 nm
Bandwidth (FWHM)	0.1 nm
Total pulse energy[a]	150 mJ
Pulse length (FWHM)[b]	16 ps
rms spot size	$34 \times 38\ \mu m$
Electrons	
Repetition rate	10 Hz
Energy	116 MeV
rms energy spread	0.2%
Beam charge	800 pC
Bunch length (FWHM)	16 ps
rms spot size	$23 \times 42\ \mu m$
rms normalized emittance	4×8 mm mrad

[a]Energy in 100 μm aperture and 16 ps FWHM main pulse: 22 mJ. See text for details.
[b]Based on models of frequency conversion.

D. J.Gibson, *et al., Phys. Rev. ST-AB*, **13**, 070703 (2010)

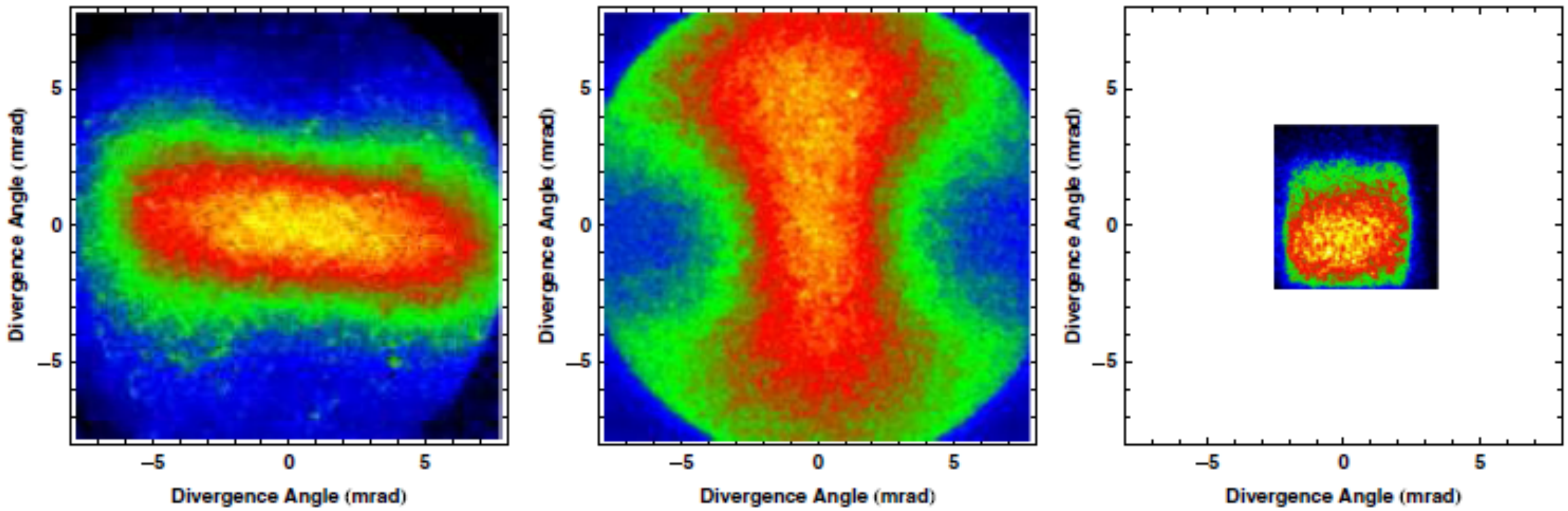

FIG. 10. (Color) γ-ray beam profiles from scintillator-coupled CCD cameras for the three laser frequencies. The beam energies are: left—295 keV (128.4 MeV + 1ω), center—466 keV (114 MeV + 2ω), and right—906 keV (130 MeV + 3ω).

TABLE III. Gamma source performance parameters.

Photons per interaction	1.6×10^5
Peak (on-axis) energy	478 keV
rms energy spread	12%
Repetition rate	10 Hz
Peak (on-axis) brightness	$1.5 \times 10^{15}\ \frac{\text{photons}}{\text{mm}^2\ \text{mrad}^2\ \text{s}\ 0.1\%\ \text{BW}}$
Inferred rms spot size	$\sim 36\ \mu\text{m}$
Beam divergence	10×6 mrad

High Power Optical Cavities

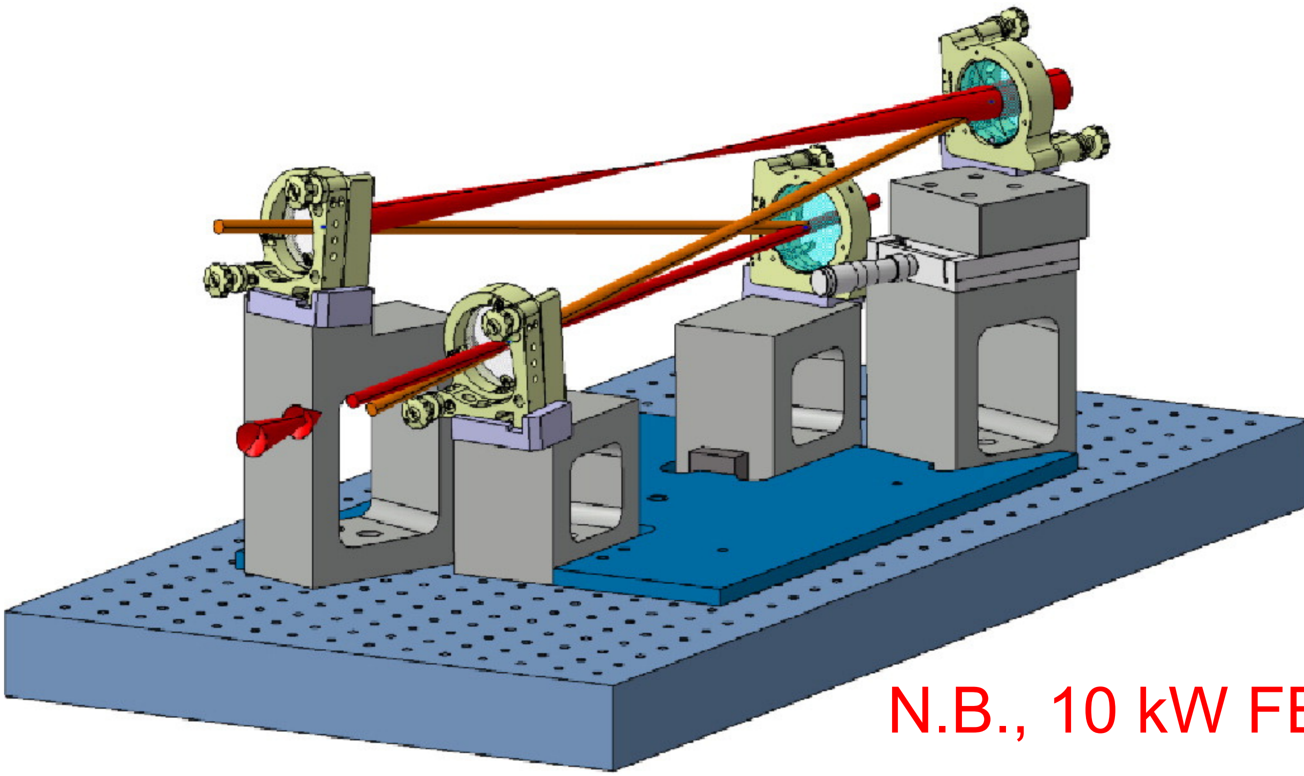

V. Brisson, *et al.*, *NIM A*, **608**, S75 (2009)

N.B., 10 kW FEL there, sans spot!

In this paper we described our first results on the locking of a Ti:sapph oscillator to a high finesse FPC. For the first time, to our knowledge, we demonstrate the possibility of stacking picosecond pulses inside an FPC at a very high repetition rate with a gain of the level of 10000. By studying the stability of four-mirrors resonators, we developed a new promising nonplanar geometry that we have just started to study experimentally. Finally, we mentioned that we shall next use the recent and powerful laser fiber amplification scheme to reach the megawatt average power inside FPC as required by the applications of the Compton X and gamma ray sources.

LAL/Thales THomX

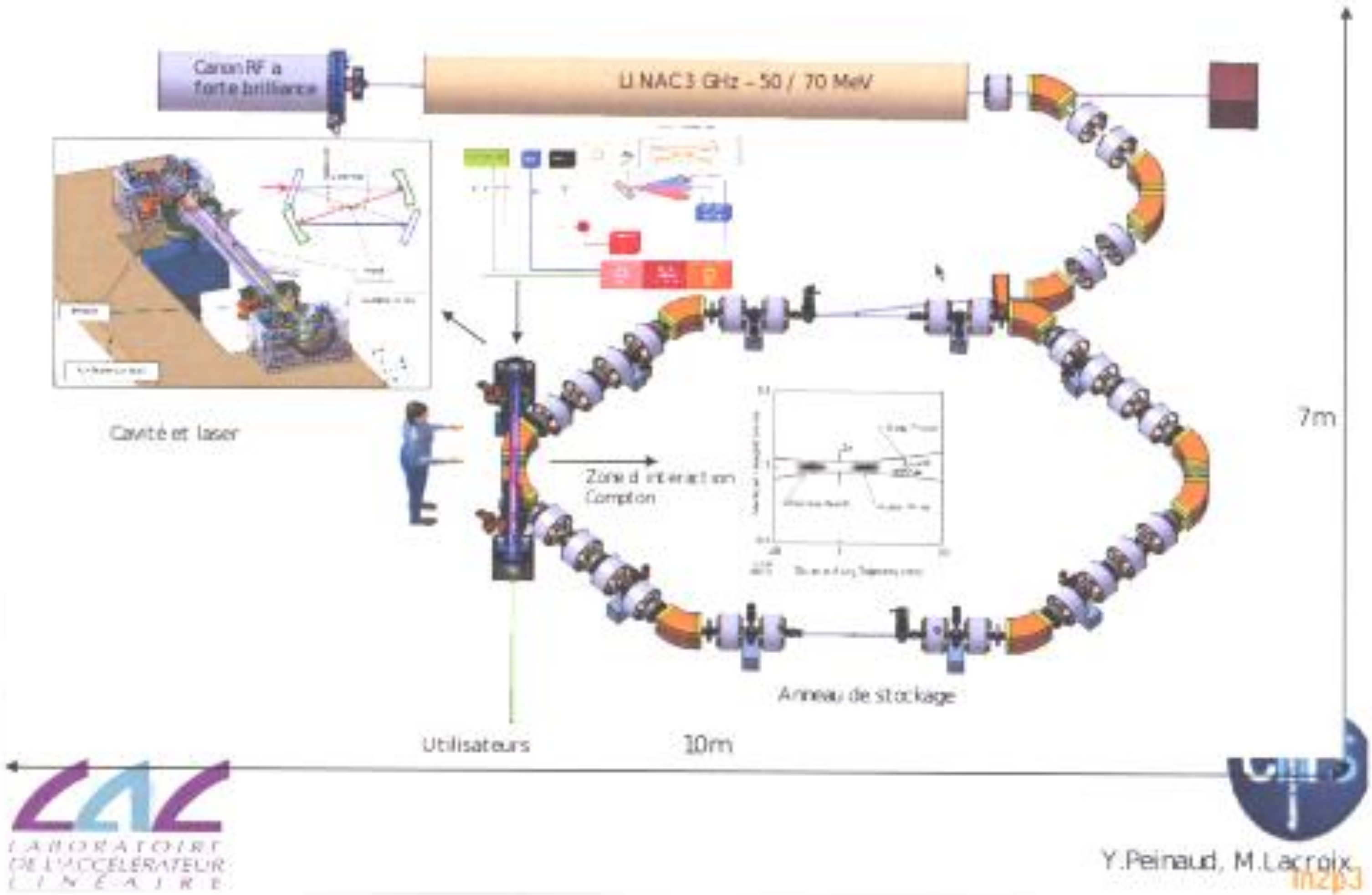

BES Workshop on Compact Light Sources (2010)

Hajima, et al.

Uranium Detection

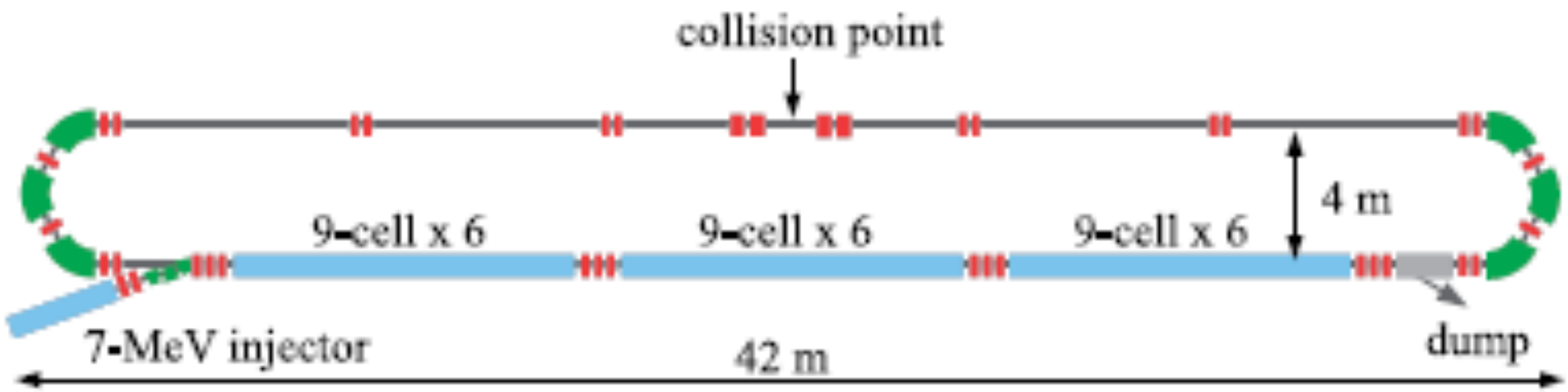

Fig. 3. Layout of the 350-MeV ERL designed for a high-flux γ-ray source. An electron beam generated by the 7-MeV injector is accelerated up to 350 MeV by the main linac and transported to the recirculation loop. The collision point for LCS γ-ray generation is located in the middle of the straight section.

Hajima, *et al., NIM A*, **608**, S57 (2009)
TRIUMF Moly Source?

Table 1
Design parameters of a high-flux γ-ray facility.

Electron beam	
Maximum energy	350 MeV
Current	13 mA
Bunch charge	100 pC
Normalized emittance (x/y)	2.2/1.0 mm–mrad
Laser and laser supercavity	
Laser	1.8 μJ, 1064 nm
Repetition rate	130 MHz
Supercavity gain	3000
γ-ray	
Total flux	1.0×10^{13} ph/s

In the design, we consider a laser supercavity that stores an intracavity laser power of 700 kW (1.8 μJ, 130 MHz, gain of 3000, Rayleigh length of 1.1 cm). The γ-ray flux in the above-mentioned

MIT CUBiX

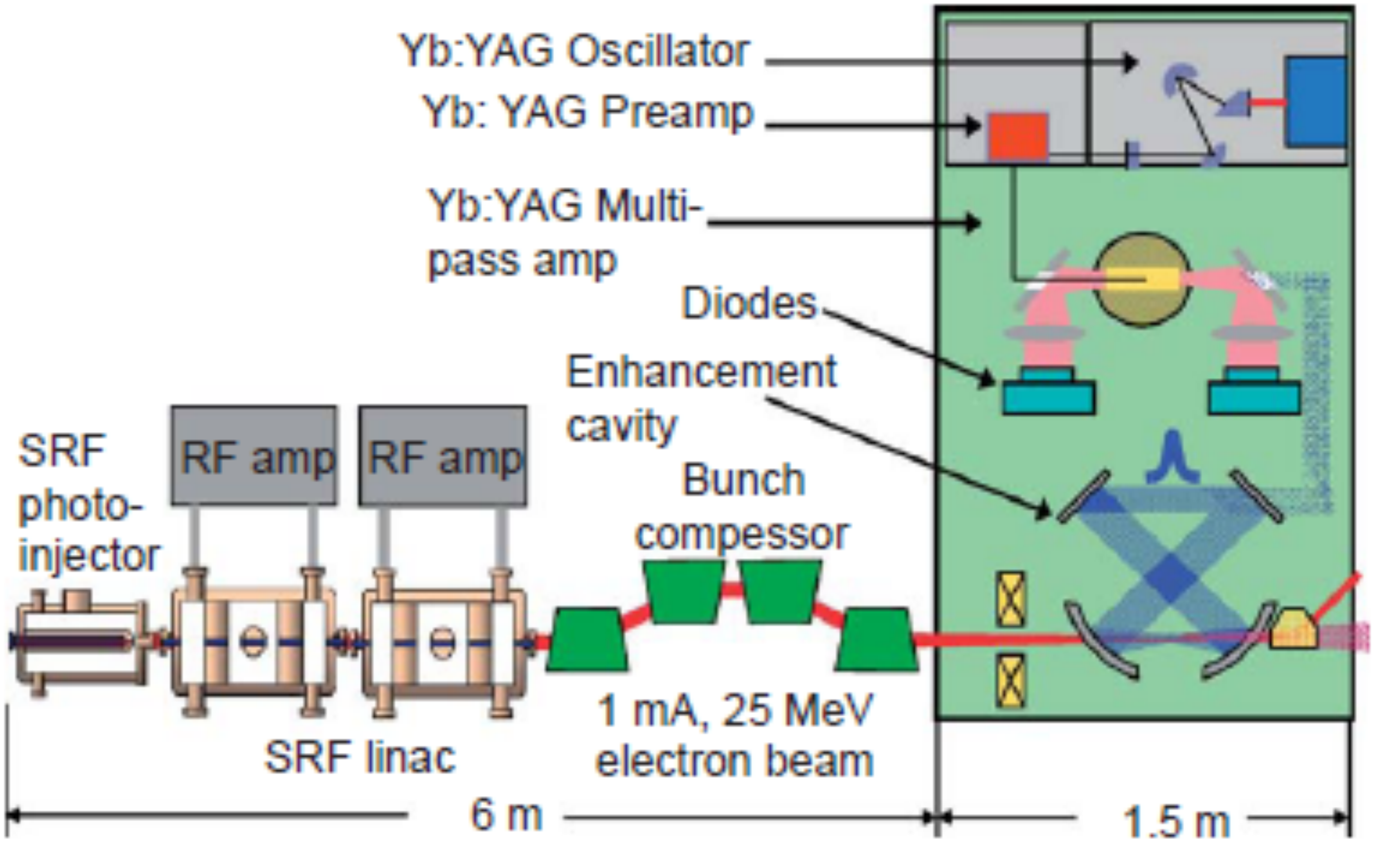

Fig. 2. Major technical components including cryocooled high-power laser and SRF linac.

Graves, *et al.*, *NIM A*, **608**, S103 (2009)

Table 1
X-ray parameters.

Parameter	Single shot	High flux
Tunable photon energy (keV)	3–30	
Pulse length (ps)	2	0.1
Flux per shot (photons)	1×10^{10}	3×10^{6}
Repetition rate (Hz)	10	10^{8}
Average flux (photons/s)	1×10^{11}	3×10^{14}
On-axis bandwidth (%)	2	1
RMS divergence (mrad)	5	1
Source RMS size (mm)	0.006	0.002
Peak brilliance (photons/(s mm^2 mrad^2 0.1%bw))	6×10^{22}	6×10^{19}
Average brilliance (photons/(s mm^2 mrad^2 0.1%bw))	6×10^{11}	2×10^{15}

numerical simulation results assuming parameters of $E = 25\,\text{MeV}$, $\varepsilon_{nx} = 0.1\,\mu\text{m}$, $x_e = 2\,\mu\text{m}$, $\Delta t_L = 0.3\,\text{ps}$, $\lambda = 1\,\mu\text{m}$, $Q_e = 10\,\text{pc}$, and $W_\gamma = 10$ mJ. Note that no nonlinear effects were included in this

Quarter Wave SRF Injector

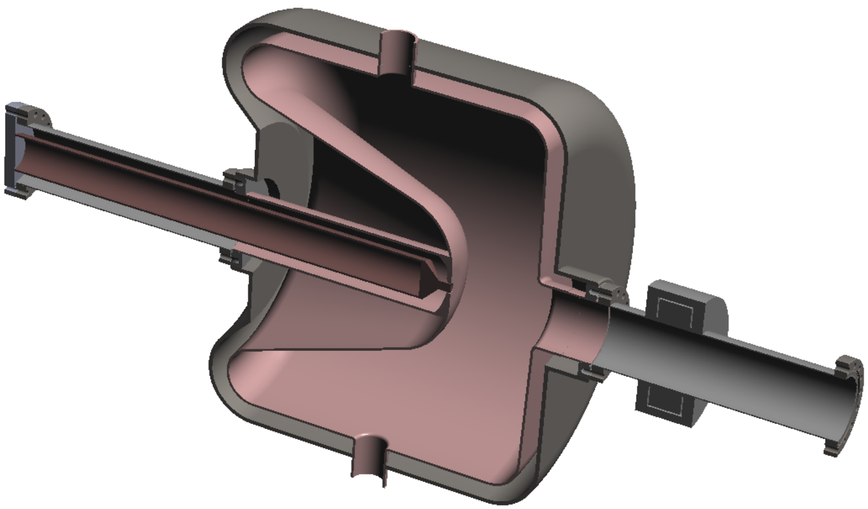

Developed in collaborations with
Niowave Inc, UW-Madison,
Naval Postgraduate School

SRF Injector Parameters	
Energy gain [MeV]	4
RF frequency [MHz]	176
Average current [mA]	1
Operating temperature [K]	4.2
RF power [kW]	5
Peak wall E-field [MV/m]	55
Peak wall B-field [mT]	105
Accelerating E-field [MV/m]	32
Cathode E-field [MV/m]	45

G. A. Krafft, CUBiX NSF Review (2010)

4K SRF CW Linac

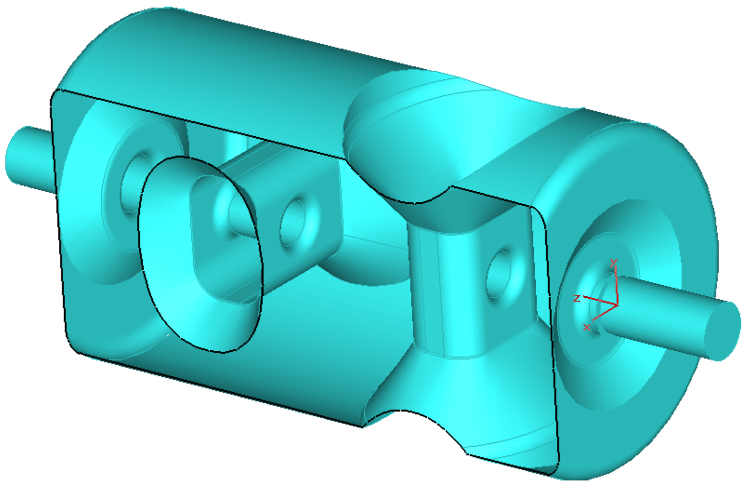

SRF Linac Parameters	
Energy gain [MeV]	25
RF frequency [MHz]	352
Average current [mA]	1
Operating temperature [K]	4.2
RF power [kW]	30

Jean Delayen developing cavities at newly formed Center for Accelerator Science at Old Dominion University (Chris Hopper of ODU/CASA) has a velocity-of-light design

4 K SRF Technology: Spoke cavities

Lower RF frequency => 4K operation

More compact for given frequency

Good mechanical rigidity

Moderate gradient (10 - 12 MV/m CW)

Longitudinal Compression Ideas

- Transverse displacement

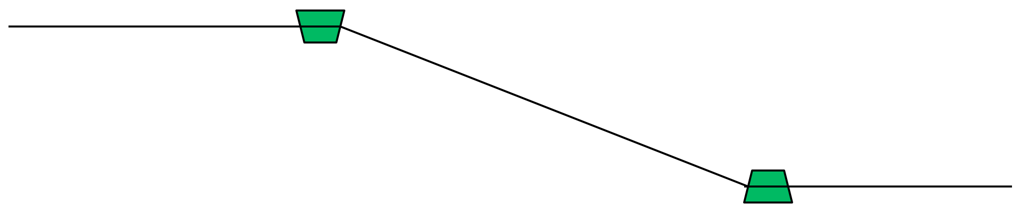

- Modified chicane

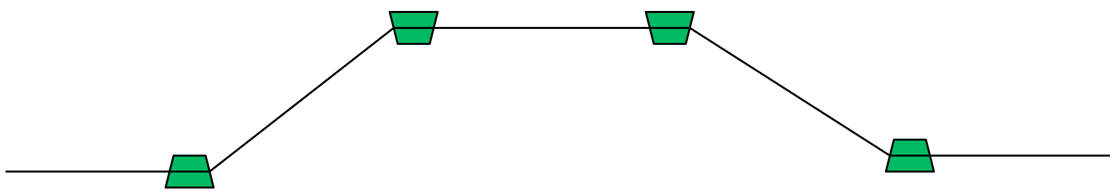

- Modified "π" bend

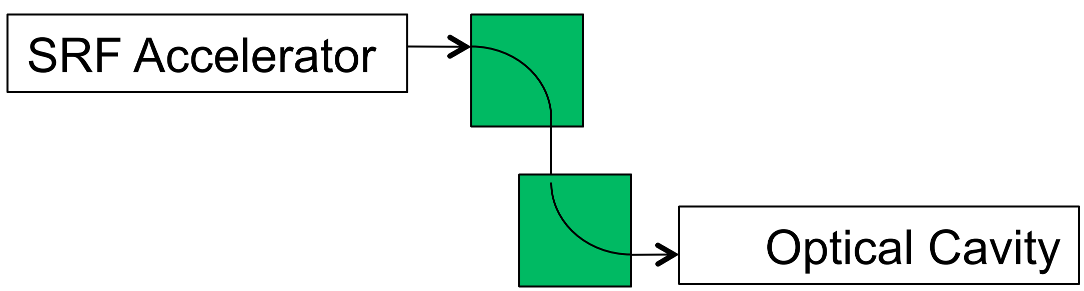

SPARC

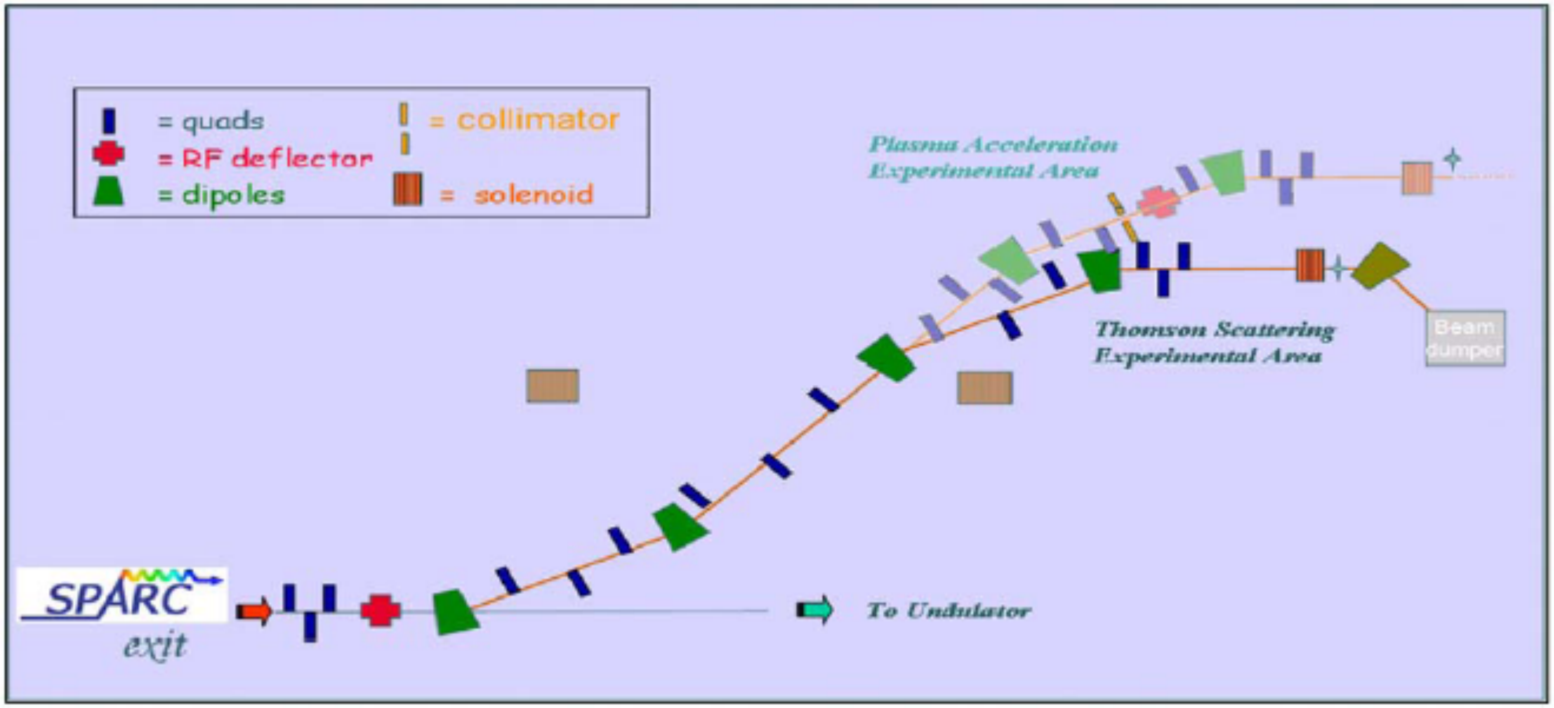

Fig. 1. Lay-out of the dog-leg like electron beam line for the TS experimental area.

A. Bacci, *et al., NIM A*, **608**, S90 (2009)

Table 1
Electron beam at the interaction point.

Parameter	Value
Bunch charge (nC)	1–2
Energy (MeV)	28–150
Length (ps)	15–20
$\varepsilon_{n\_x,y}$ (mm-mrad)	1–5
Energy spread (%)	0.05*–0.2
Spot size at interaction point rms (μm)	5–10

Conclusions

- Compton sources of high energy photons have existed for about thirty years
- The have followed the usual progression: [1] borrow an existing machine (1^{st} generation), and [2] make it better by technological innovation (2^{nd} generation?)
- We are perhaps approaching 3^{rd} generation devices, i.e., accelerators specifically designed for Compton/ Thomson sources.
- Expect “convergence” with high energy collider design ideas
- Lots of ideas, but still looking for the “killer app”.

Conclusions

- A “new” calculation scheme for high intensity pulsed laser Thomson Scattering has been developed. This same scheme can be applied to calculate spectral properties of “short”, high-K wigglers.
- Due to ponderomotive broadening, it is simply wrong to use single-frequency estimates of flux and brilliance in situations where the square of the field strength parameter becomes comparable to or exceeds the ($1/N$) spectral width of the induced electron wiggle
- The new theory is especially useful when considering Thomson scattering of tabletop TeraWatt lasers, which have exceedingly high field and short pulses. Any calculation that does not include ponderomotive broadening is incorrect.

Accelerators in Medicine

Todd Satogata
Jefferson Lab, Old Dominion University
(With some slides from Jean Delayen)

NASA Space Radiation Laboratory (BNL)

- Long-range space travelers (e.g. to Mars) are exposed to high radiation doses
- Most concern is about heavy ions from galactic cosmic rays
- Less expensive to simulate/ study on earth
  - 200-800 MeV/u ions
- Biological effects of high radiation doses of this type are controversial
  - DNA damage, repair
  - Mutagenesis
  - Carcinogenesis
  - Cellular necrosis
- Radiation also kills cancers

X-Ray Cancer Therapy

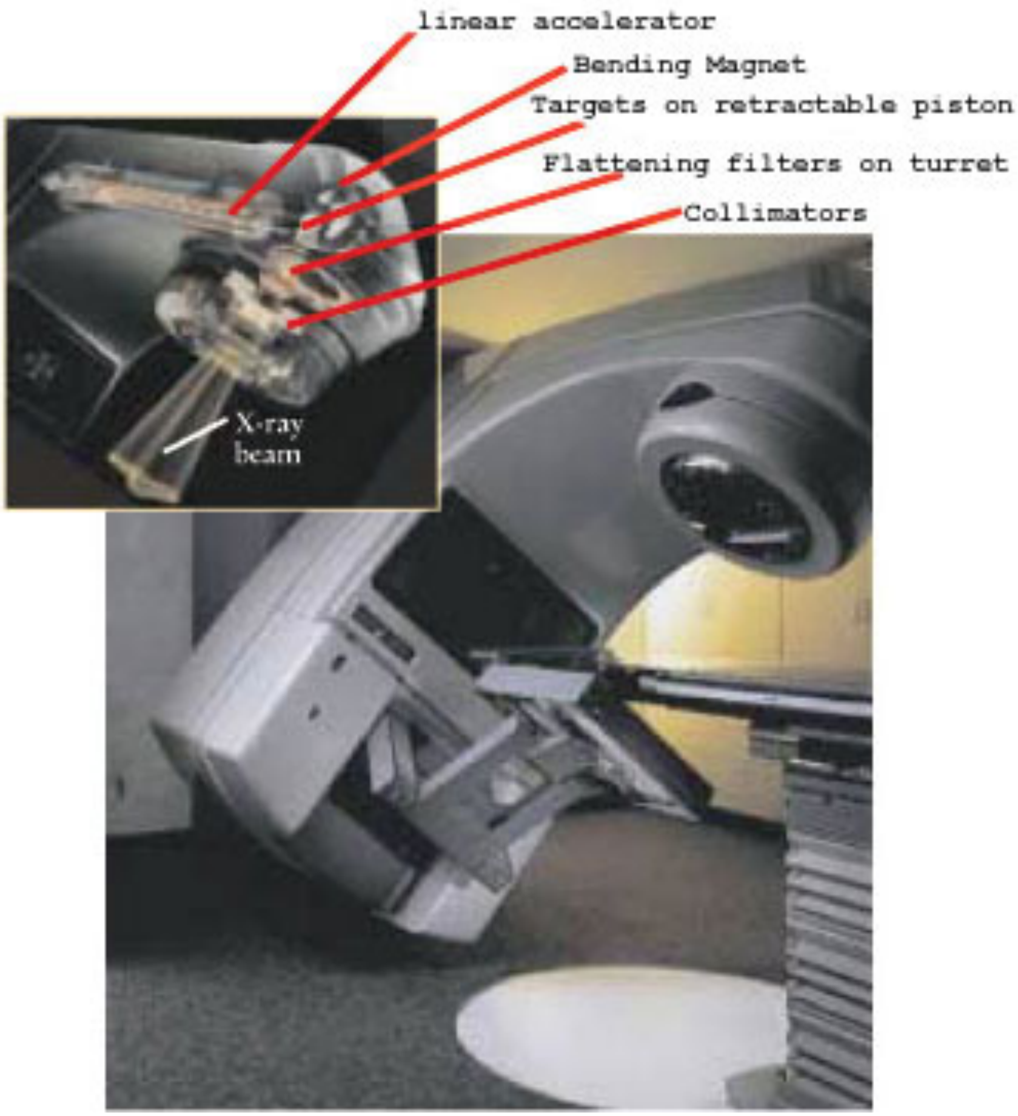

- Conventional X-ray cancer treatment accelerators are "small"
  - Single room "facility"
  - 5-25 MeV X-rays
    - x100 diagnostic X-ray
  - Generated by a small linac or a betatron
    - A few MV/m
  - 500+ US locations

- Treatment planning and beam shaping are challenging on patient-by-patient basis
  - Multiple angles, IMRT

X-Ray IMRT

- X-ray intensity-modulated radiation therapy (IMRT)
  - “Commonly performed”
  - Requires multiple fields
- Can (mostly) avoid critical structures
  - But still residual dose
  - Residual dose is high on skin, in early entry areas
- X-ray radiotherapy is
  - Less expensive...
  - But not necessarily better

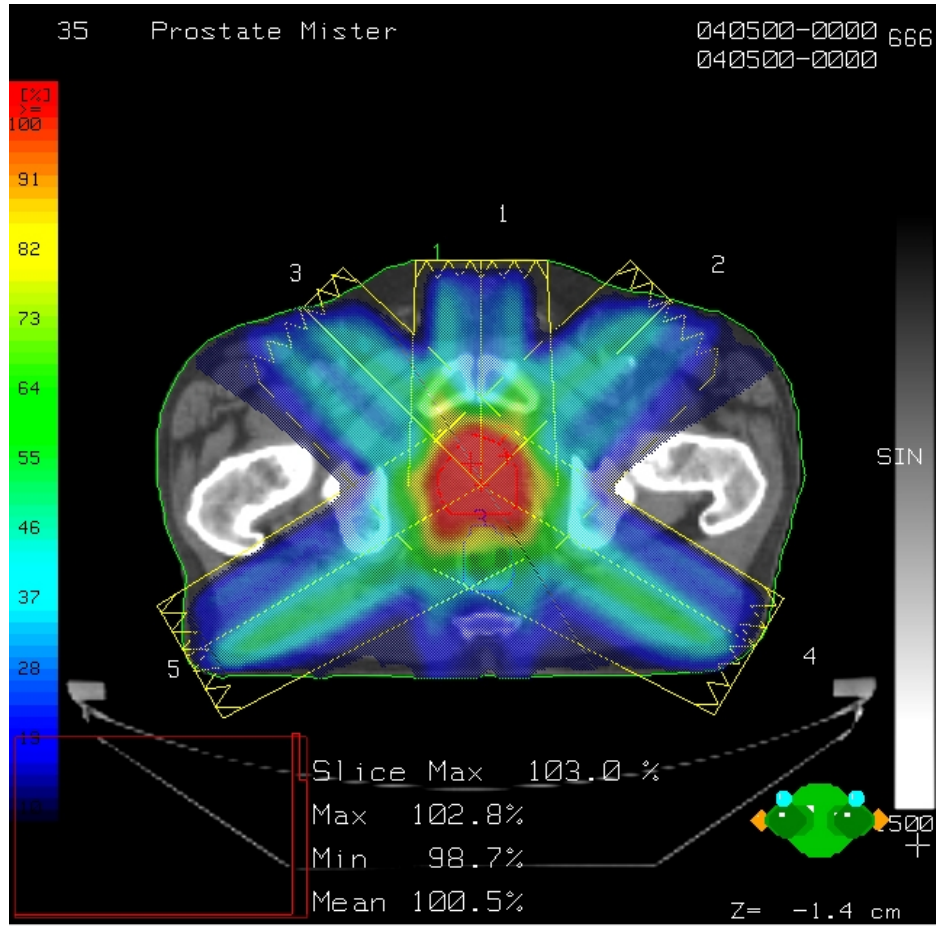

Image courtesy of Varian/Eclipse Advertising

X-Rays vs Protons

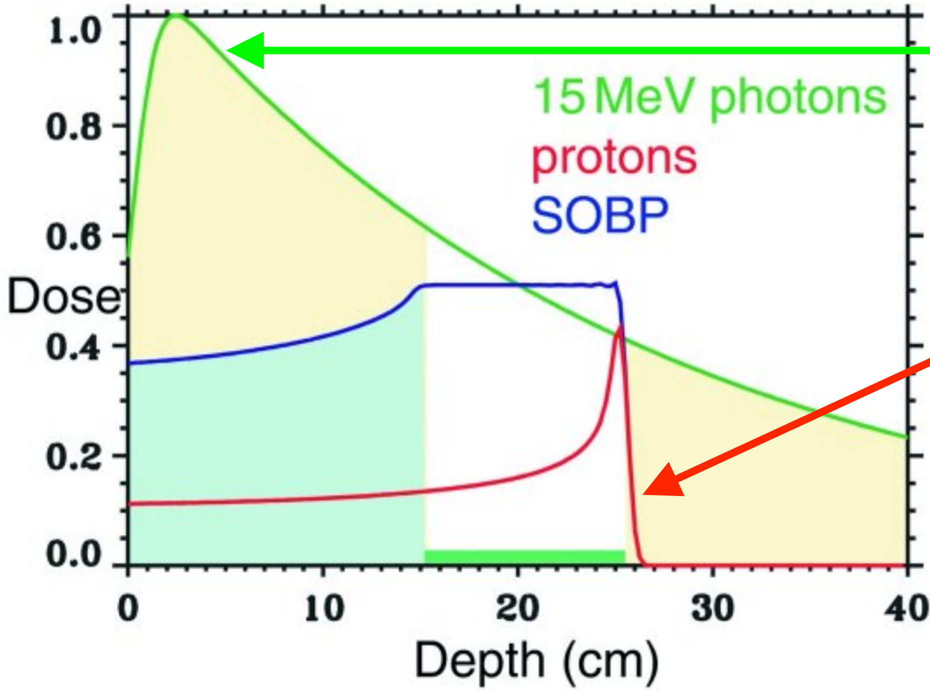

X-rays deposit most of their dose near the surface (skin) of the patient

Most proton dose is deposited in the sharp "Bragg Peak", with no dose beyond

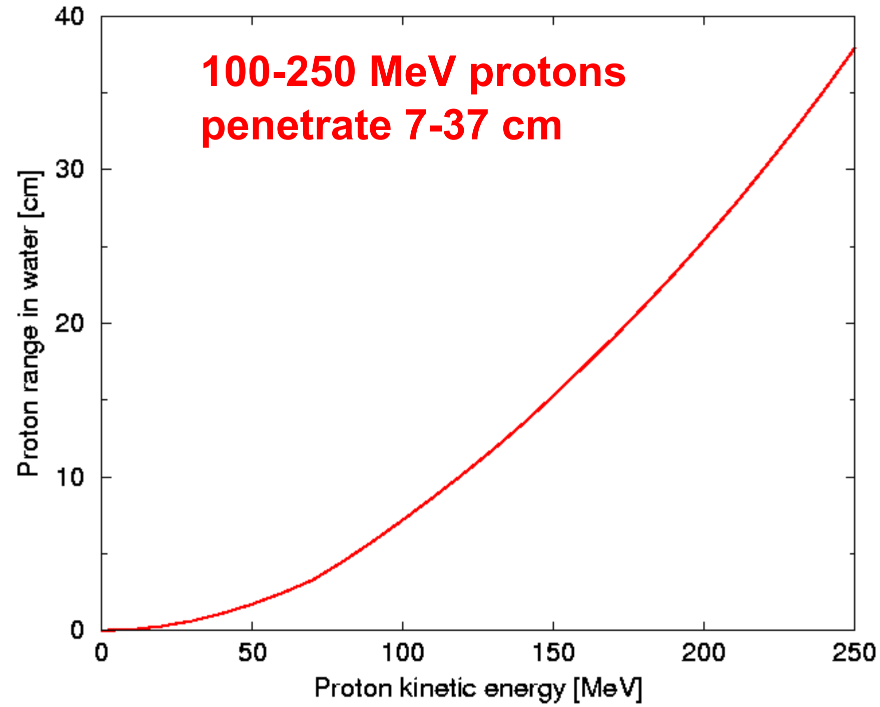

Scanning the proton energy makes a Spread Out Bragg Peak (SOBP) that spans the depth of the tumor

Carbon and other light hadrons also work

- Even sharper Bragg peak
- Nuclear dissociation, larger tail dose

X-Rays vs Protons

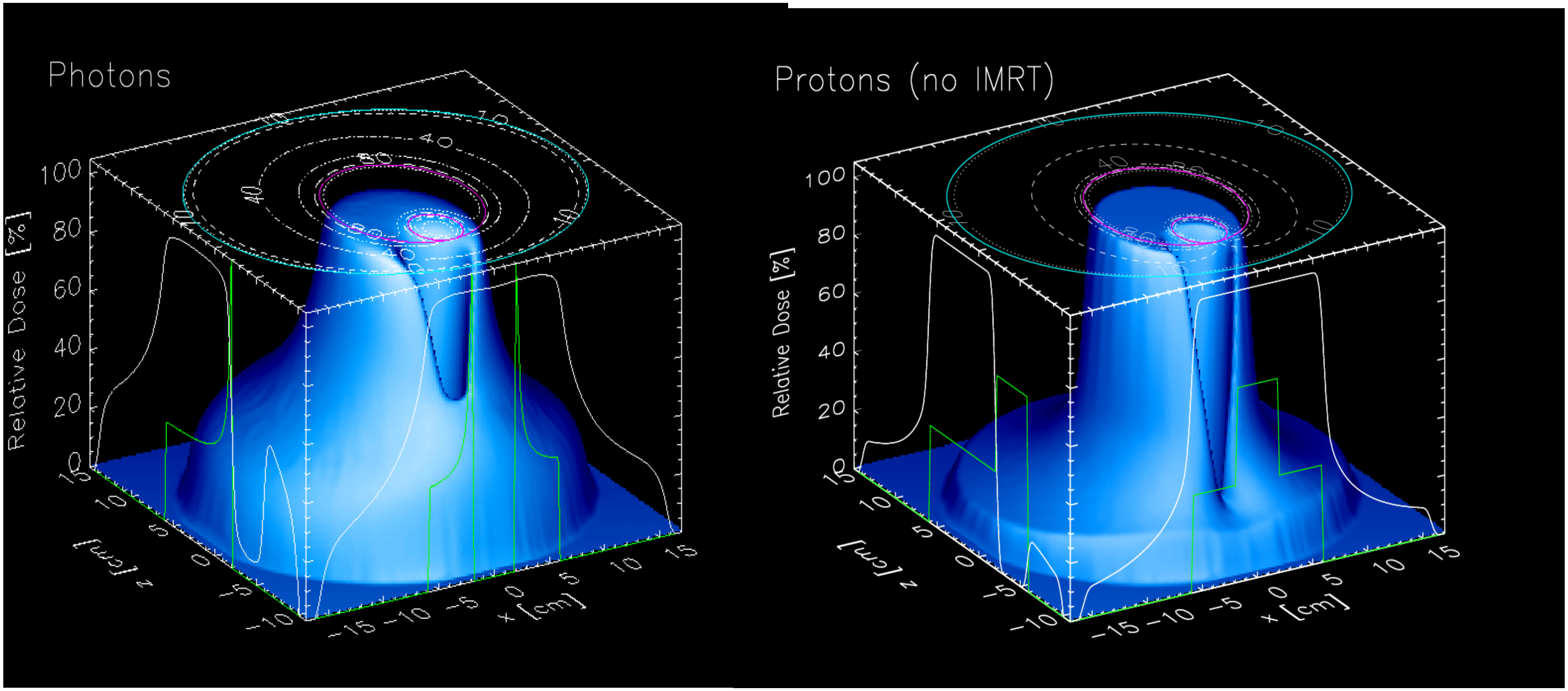

- With multiple angles/fields, protons excel even better
  - The “spine” is better protected
  - Dose to surrounding (healthy) tissues is intrinsically lower

Cancer Therapy Accelerators

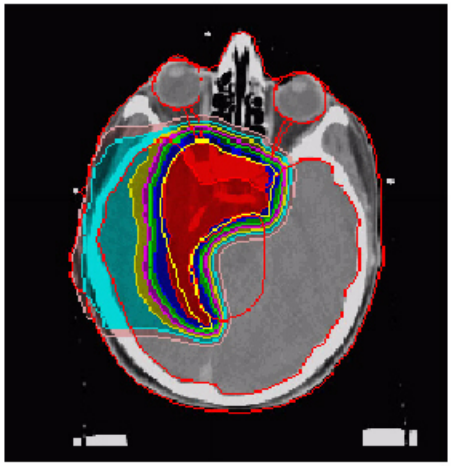

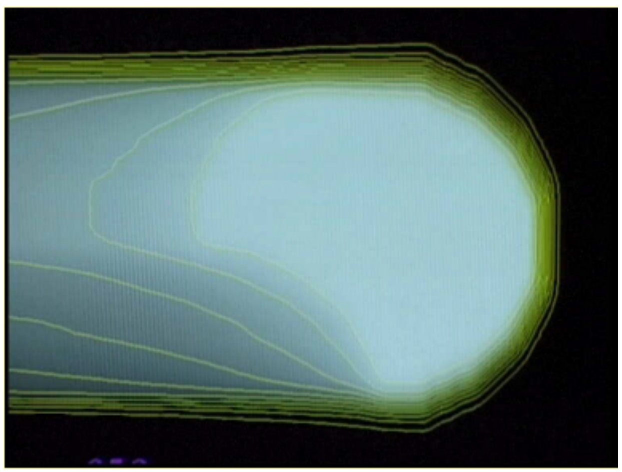

Images courtesy of Paul Scherrer Institute

- X-rays, protons, and light ion beams are all used worldwide in modern cancer radiotherapy
- Need to minimize side-effects
  - Minimize dose to healthy tissue
  - But dose cancer cells (>=5 krem!)
- X-rays are:
  - less expensive (>500 US locations)
  - better for peripheral/surface tumors
- Protons/Ions are:
  - more expensive (~5 US p locations)
  - better for deeper, critical tumors
  - capable of conformal spot-scanning treatment; best 3D dose localization

Ion Therapy Facilities

WHO, WHERE	COUNTRY	PARTICLE	S/C*, MAX. ENERGY (MeV)	BEAM DIRECTION	START OF TREATMENT	TOTAL PATIENTS TREATED	DATE OF TOTAL
ITEP, Moscow	Russia	p	S 250	1 horiz.	1969	4246	Dec-10
St.Petersburg	Russia	p	S 1000	1 horiz.	1975	1362	Dec-10
PSI, Villigen	Switzerland	p**	C 250	1 gantry, 1 horiz.	1996	772	Dec-10
Dubna	Russia	p	C 200****	horiz.	1999	720	Dec-10
Uppsala	Sweden	p	C 200	1 horiz.	1989	1000	Dec-10
Clatterbridge	England	p	C 62	1 horiz.	1989	2021	Dec-10
Loma Linda	CA.,USA	p	S 250	3 gantry, 1 horiz.	1990	15000	Jan-11
Nice	France	p	C 65	1 horiz.	1991	4209	Dec-10
Orsay	France	p*****	C 230	1 gantry,1 horiz.	1991	5216	Dec-10
iThemba Labs	South Africa	p	C 200	1 horiz.	1993	511	Dec-09
IU Health PTC, Bloomington	IN.,USA	p	C 200	2 gantry, 1 horiz.	2004	1145	Dec-10
UCSF	CA.,USA	p	C 60	1 horiz.	1994	1285	Dec-10
HIMAC, Chiba	Japan	C-ion	S 800/u	horiz.,vertical	1994	5497	Aug-10
TRIUMF, Vancouver	Canada	p	C 72	1 horiz.	1995	152	Dec-10
HZB (HMI), Berlin	Germany	p	C 72	1 horiz.	1998	1660	Dec-10
NCC, Kashiwa	Japan	p	C 235	2 gantry	1998	772	Dec-10
HIBMC,Hyogo	Japan	p	S 230	1 gantry	2001	2382	Nov-09
HIBMC,Hyogo	Japan	C-ion	S 320/u	horiz.,vertical	2002	638	Nov-09
PMRC(2), Tsukuba	Japan	p	S 250	gantry	2001	1849	Dec-10
NPTC, MGH Boston	MA.,USA	p	C 235	2 gantry, 1 horiz.	2001	4967	Dec-10
INFN-LNS, Catania	Italy	p	C 60	1 horiz.	2002	174	Mar-09
Shizuoka Cancer Center	Japan	p	S 235	3 gantry, 1 horiz.	2003	986	Dec-10
Southern Tohoku PTC, Fukushima	Japan	p	C 230	2 gantry, 1 horiz.	2008	no data	Dec-10
WPTC, Zibo	China	p	C 230	2 gantry, 1 horiz.	2004	1078	Dec-10
MD Anderson Cancer Center, Houston	TX.,USA	p***	S 250	3 gantry, 1 horiz.	2006	2700	Apr-11
UFPTI, Jacksonville	FL.,USA	p	C 230	3 gantry, 1 horiz.	2006	2679	Dec-10
NCC, Ilsan	South Korea	p	C 230	2 gantry, 1 horiz.	2007	648	Dec-10
RPTC, Munich	Germany	p**	C 250	4 gantry, 1 horiz.	2009	446	Dec-10
ProCure PTC, Oklahoma City	OK.,USA	p	C 230	1 gantry, 1 horiz, 2 horiz/60 deg.	2009	21	Dec-09
HIT, Heidelberg	Germany	p**	S 250	2 horiz.	2009	treatment started	Nov-09
HIT, Heidelberg	Germany	C-ion**	S 430/u	2 horiz.	2009	treatment started	Nov-09
UPenn, Philadelphia	PA.,USA	p	C 230	4 gantry, 1 horiz.	2010	150	Dec-10
GHMC, Gunma	Japan	C-ion	S 400/u	3 horiz., vertical	2010	treatment started	Mar-10
IMPCAS, Lanzhou	China	C-ion	S 400/u	1 horiz.	2006	126	Dec-10
CDH Proton Center, Warrenville	IL.,USA	p	C 230	1 gantry, 1 horiz, 2 horiz/60 deg.	2010	treatment started	Oct-10
HUPTI, Hampton	VA., USA	p	C 230	4 Gantry, 1 horiz.	2010	treatment started	Aug-10
IFJ PAN, Krakow	Poland	p	C 60	1 horiz.	2011	9	Apr-11
Medipolis Medical Research Institute, Ibusuki	Japan	p	S 250	3 gantry	2011	treatment started	Jan-11

- 38 ion therapy facilities presently in operation worldwide
- 22 more proposed or under construction
- protons are most common
- heavy ions are becoming more popular

From PTCOG website

http://ptcog.web.psi.ch/ptcentres.html

Two Leading US Proton Therapy Facilities

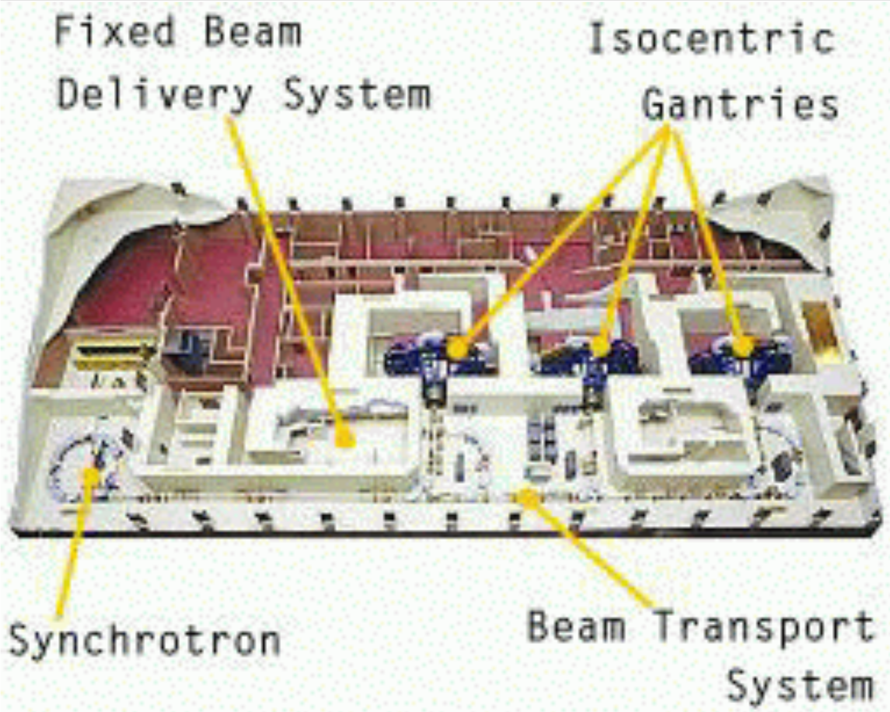

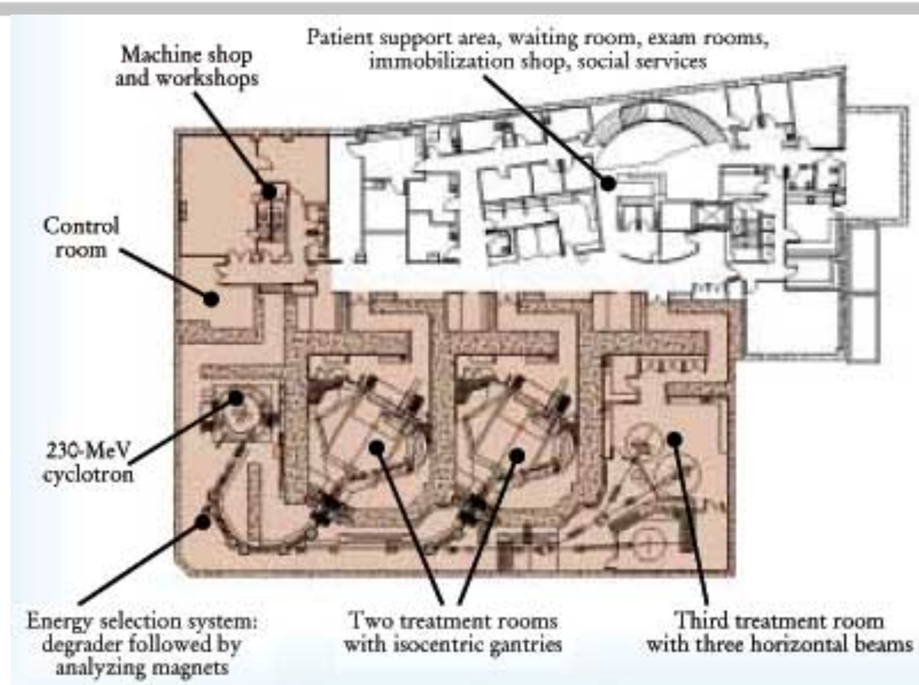

- Loma Linda (California)
  - synchrotron accelerator
  - built/commissioned at Fermilab
  - first patient: 1991
  - world-leading patient throughput
    - up to 200 patients/day

- Mass General Hospital (Boston)
  - cyclotron accelerator
  - corporate involvement from IBA
  - first patient: 2001
  - much faster coming up to speed
    - >100 patients/day

Design Decisions

- Some design decisions for proton/ion beams
  - Slow spill or fast delivery
    - Most present facilities opted for slow spill, mechanical collimation
    - A few facilities (PSI, Penn/MGH/Loma Linda) are interested in spot or continuous scanning
  - Energy variability
    - Energy degraders; simple but slow, secondary n dose
    - Variable-energy extraction: less duty factor but cleaner
  - Beam sizes
    - Larger beams, collimation: simpler but less flexible
    - Smaller beams, scanning; more complex but flexible

  - RCMS objective: simple flexibility
  - Cyclotron vs synchrotron?

Cyclotron vs Synchrotron: Cyclotron

(ACCEL superconducting cyclotron for RPTC, Munich)

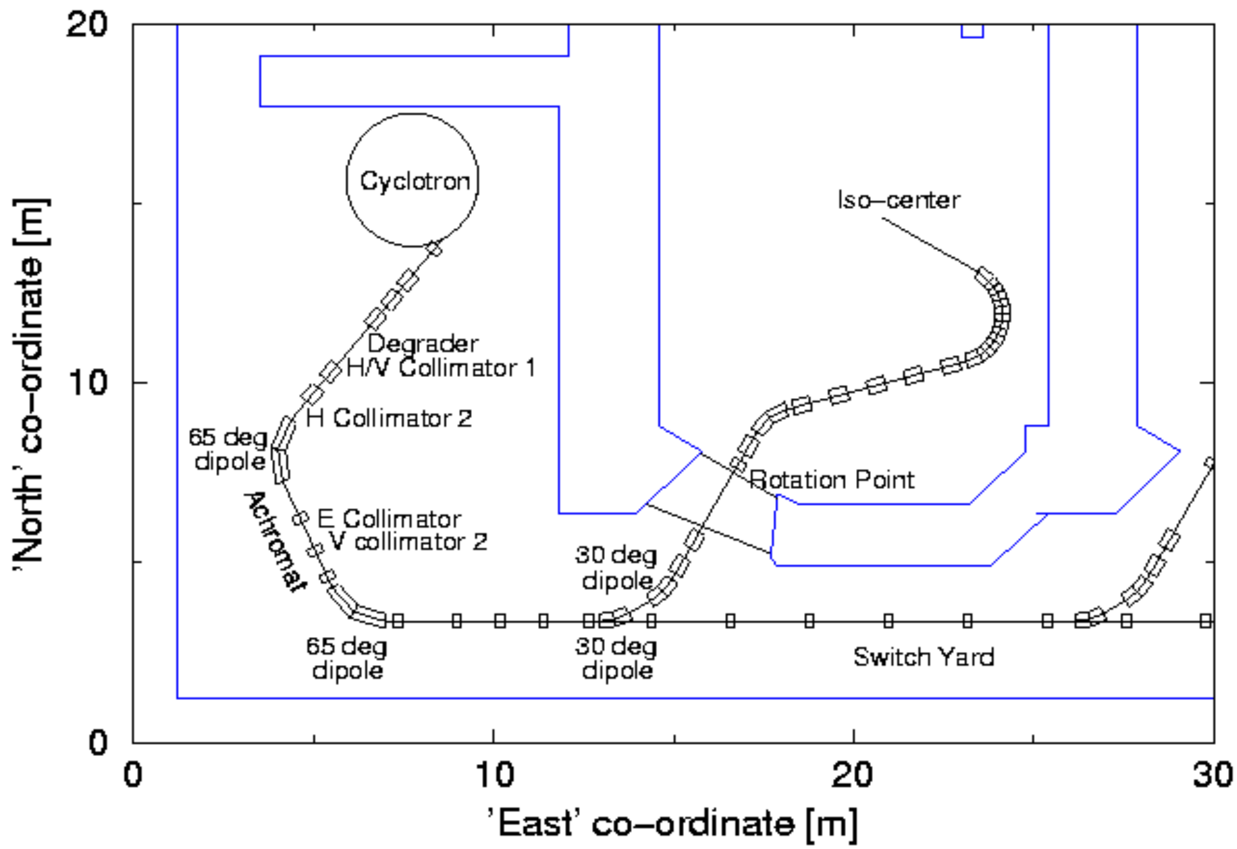

- Fixed energy output at constant current
- Energy degrader reduces beam energy
- Collimators scrape beam to size
  - secondary n dose
- Large intrinsic beam size in all three dimensions

Cyclotron vs Synchrotron: Synchrotron

(Rapid Cycling Medical Synchrotron, RCMS)

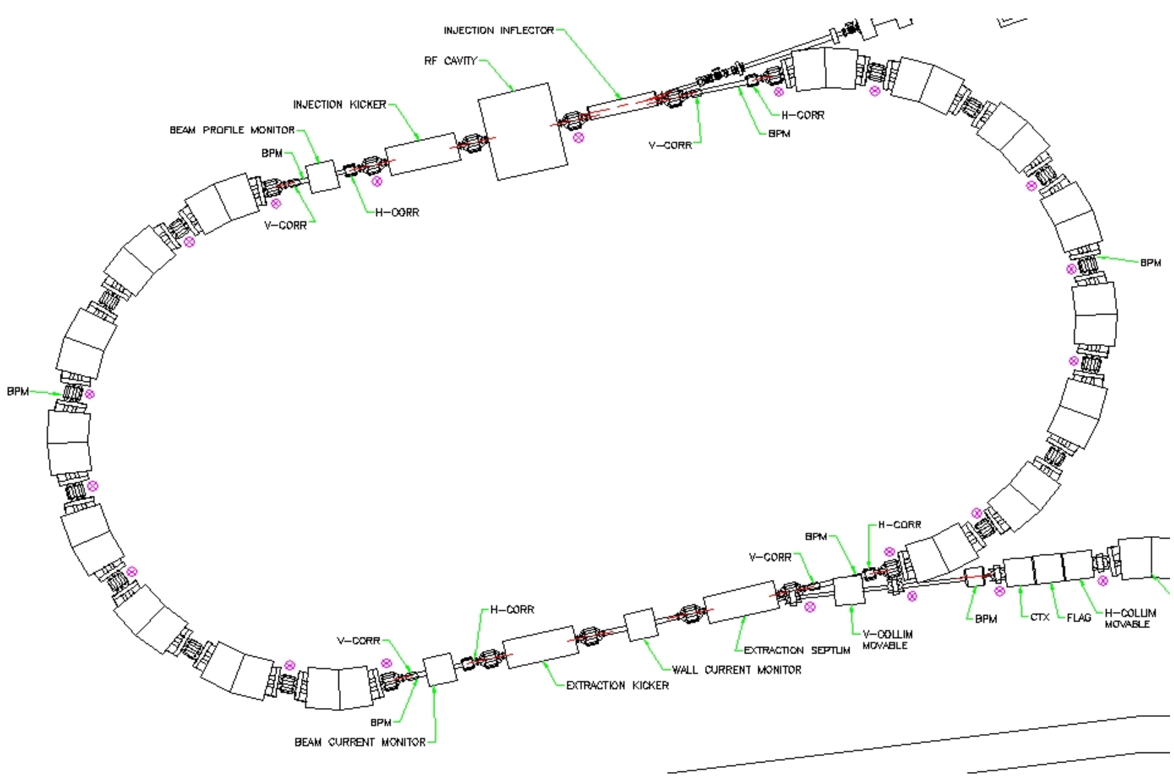

- Accelerate variable beam intensity to variable energy
  - 50-250 MeV
  - No energy degrader
  - Smaller beam sizes
- Accelerate either
  - Small beam intensity rapidly (30-60 Hz), extract in one turn (RCMS)
  - Large beam intensity slowly, extract in many turns (LLUMC)

Rapid Cycling Medical Synchrotron

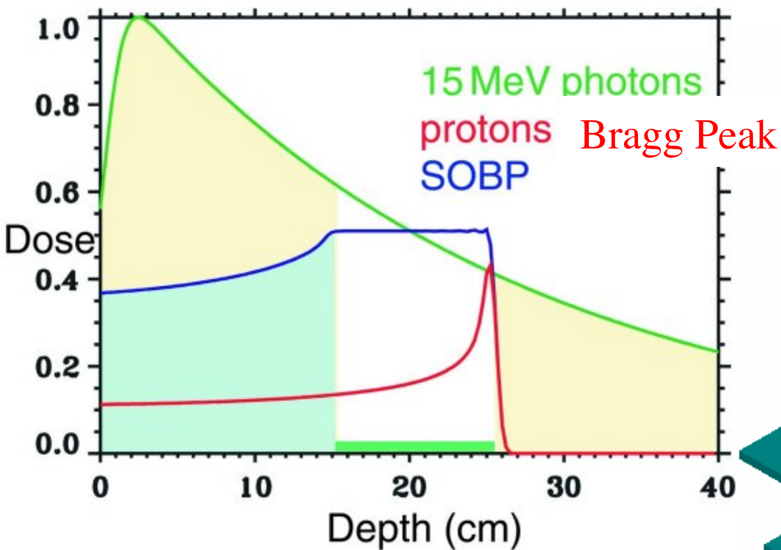

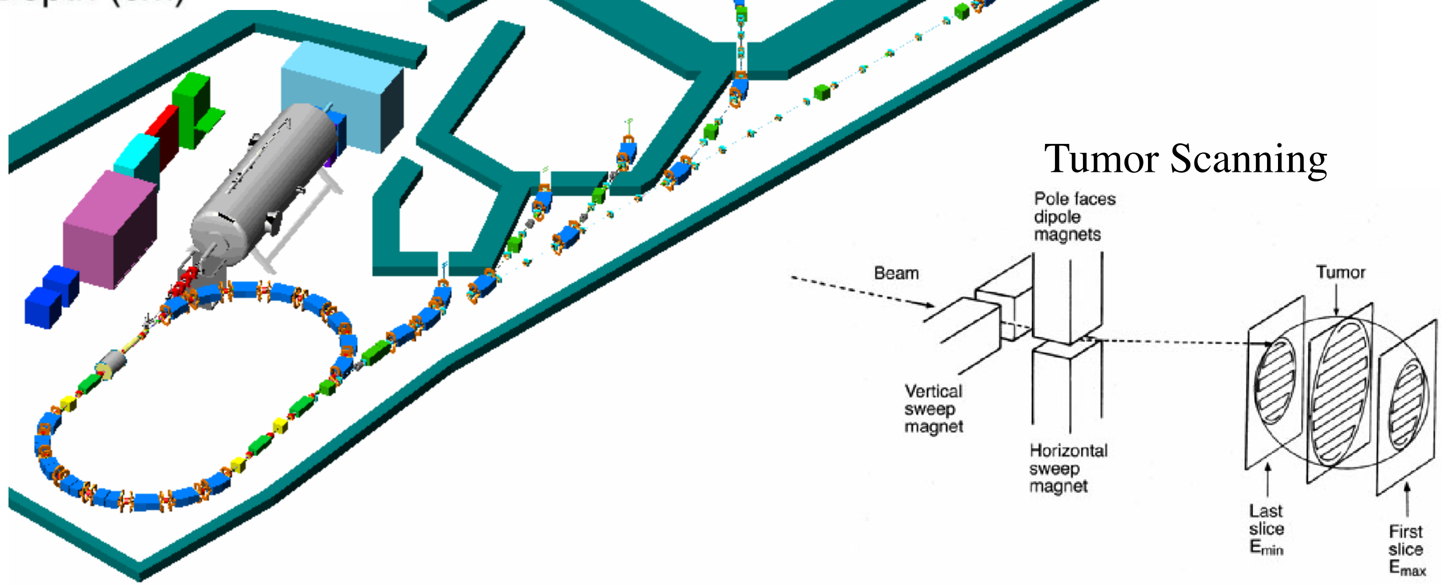

An RCMS Facility

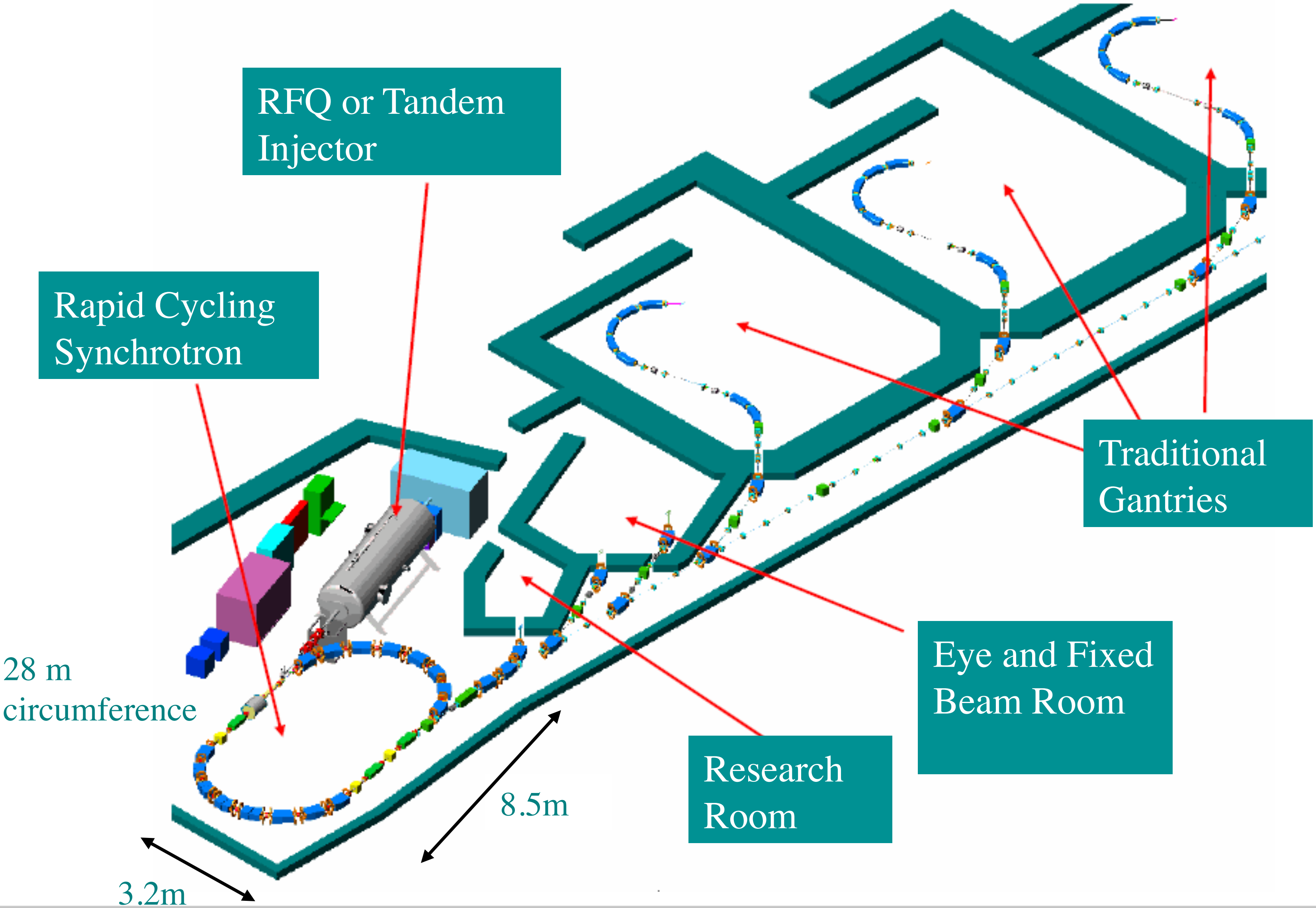

MGH Gantry

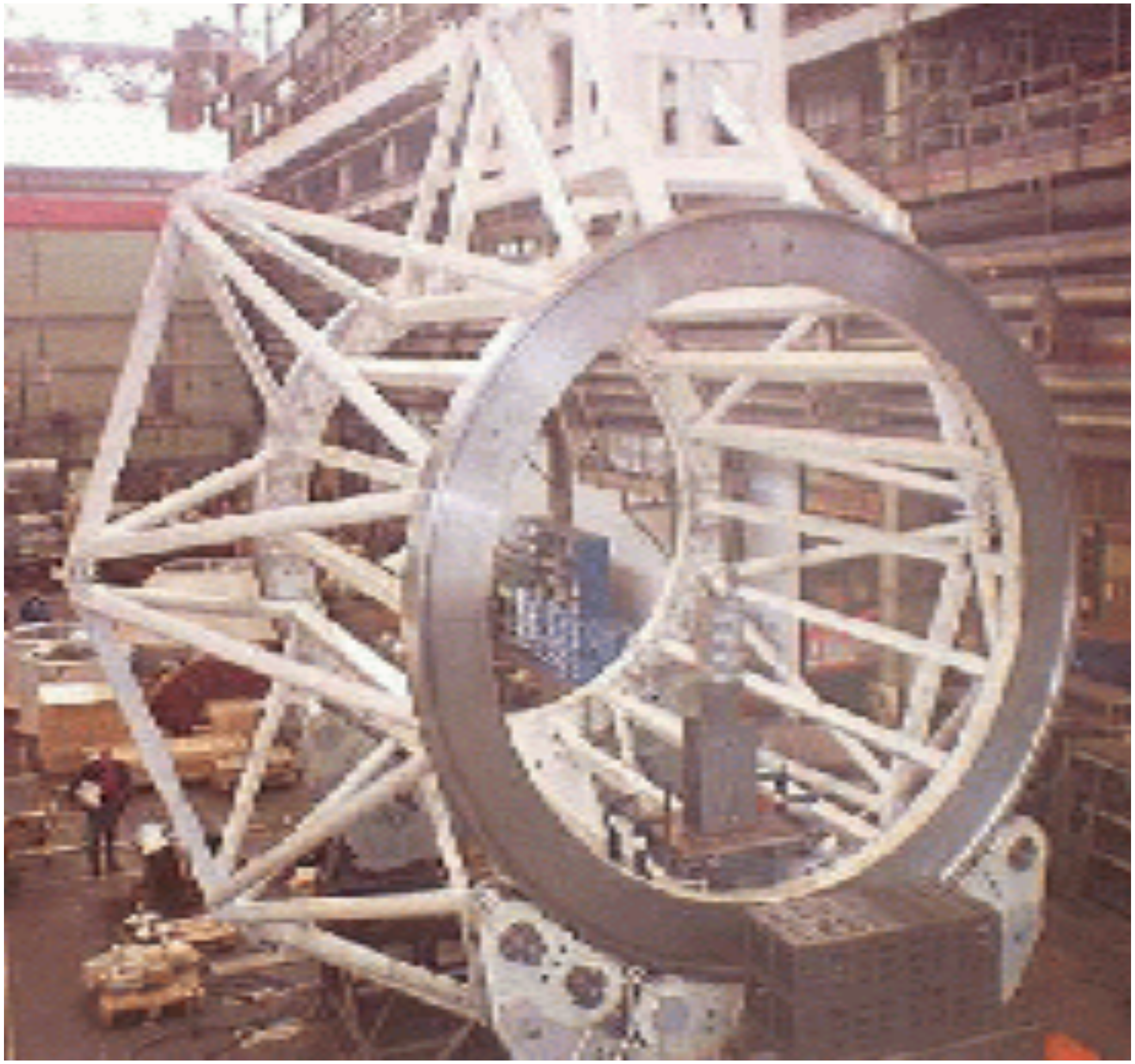

Courtesy of J. Flanz

- Up to 250 MeV p
- 1mm tolerances
- ~200 tons
- Gantries can dominate facility

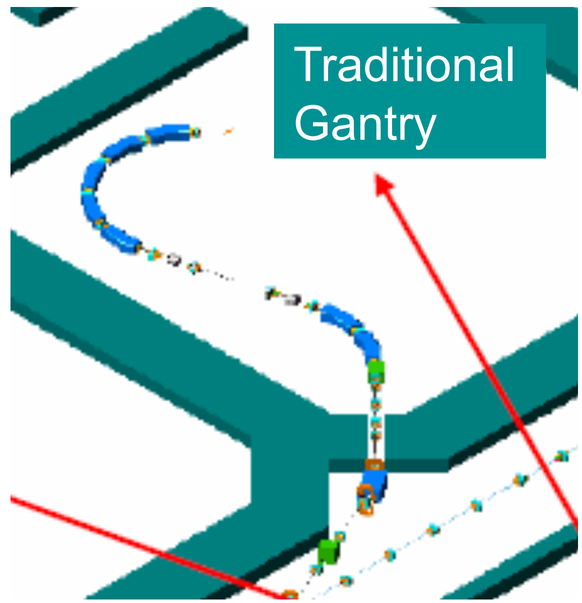

FFAG Gantries

- FFAG gantries are an excellent fit to the RCMS concept:
  - Very strong focusing
    - magnet ID down to as low as 2 cm
  - Many very short magnets
    - leverage simpler production, permanent magnets
  - Large momentum acceptance
    - no gantry magnet changes for 90-250 MeV protons
  - Compatible with iron-free superconducting magnets
    - leverage BNL world expertise in direct-wind magnets

  - Low weight of small-aperture iron-free magnets
    - ~50 kg/magnet (!)
    - Total gantry beamline magnet weight ~1500 kg (!!!)

Courtesy of D. Trbojevic

Permanent Magnet FFAG Gantry

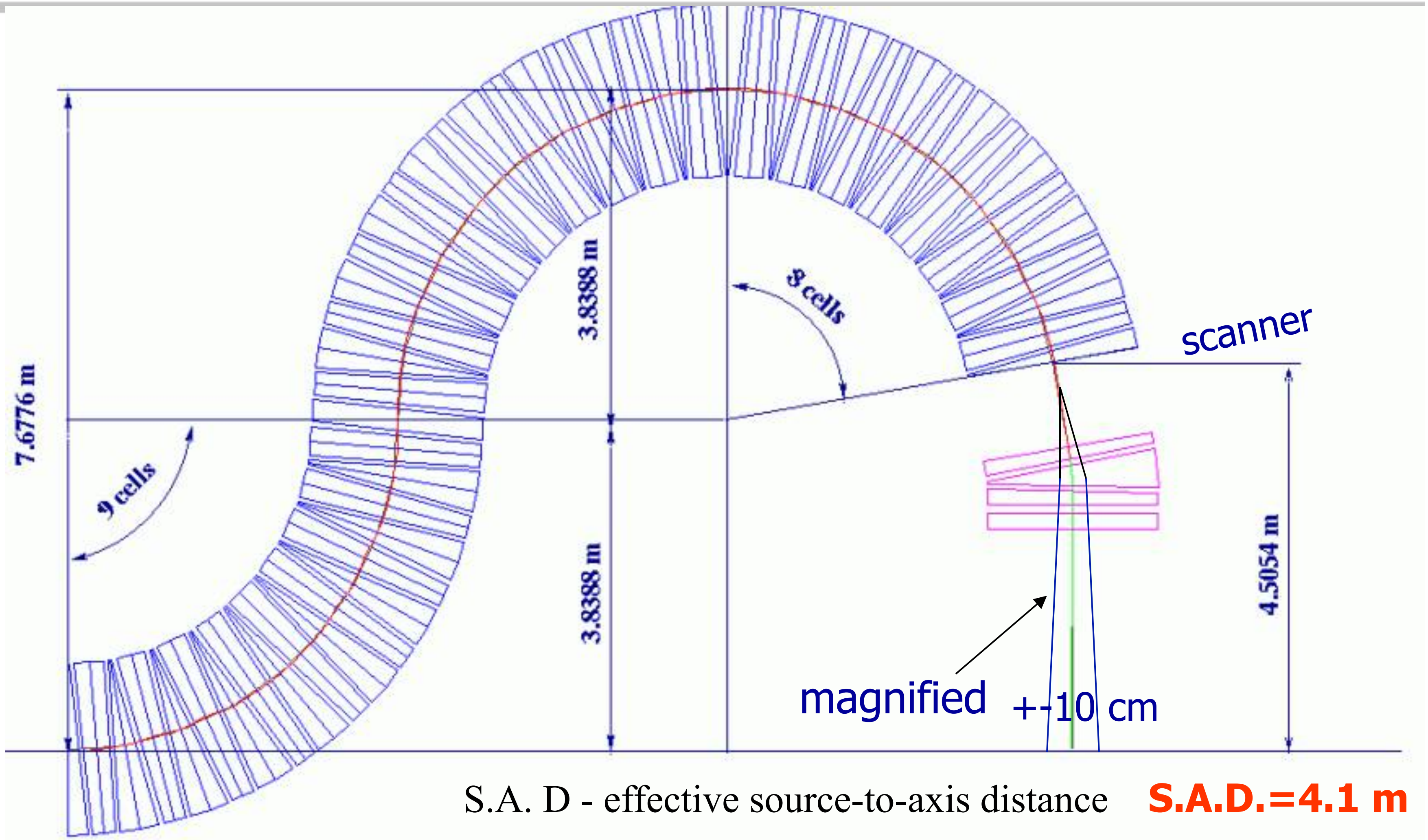

S.A. D - effective source-to-axis distance **S.A.D.=4.1 m**

$L_{\_BD}$ = 25 cm, GD =-33.7 T/m, B_{max}= 1.5 T + 33.7 T/m*0.012 mm = 1.9 T
$L_{\_BF}$ = 30 cm, GF =+35.5T/m, B_{max}=-0.25 T -+ 35.5 m*0.028 mm = 1.2 T

Courtesy of D. Trbojevic

Superconducting (SC) Gantry Magnets

SC magnets + small beam size = practical light gantries

New SC magnets are light and strong

- Iron-free (coil dominated fields)
- Solid state coolers (no He)
- Field containment
- “Direct wind” construction

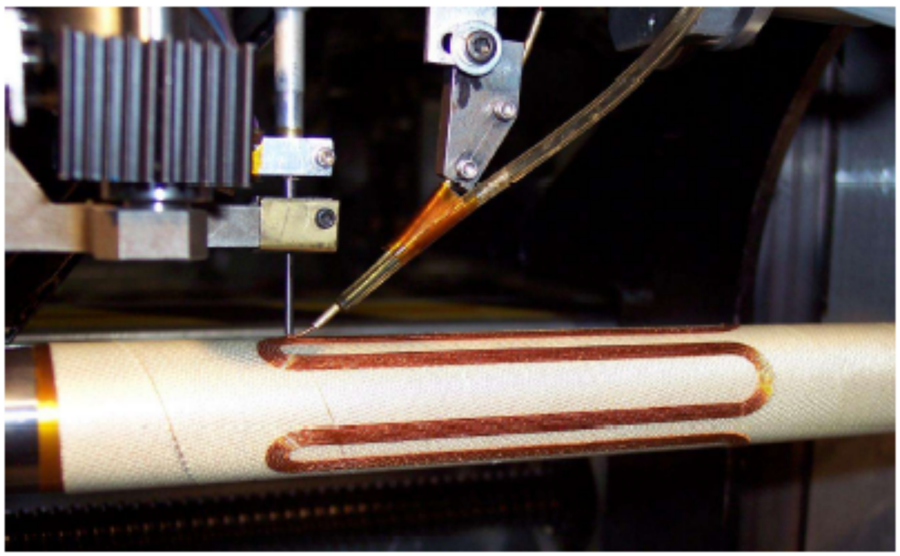

World’s first “direct wind” coil machine at BNL

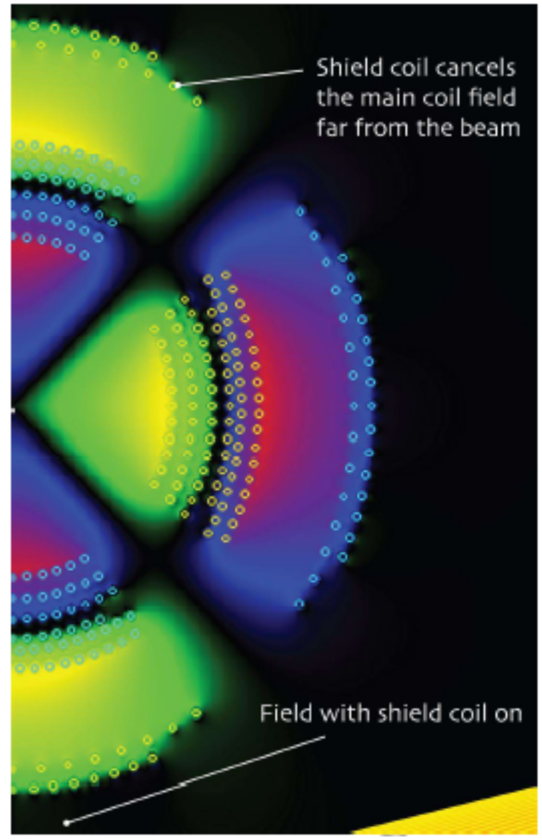

Linear Collider magnet

Courtesy of B. Parker

SC Magnet Non-Scaling FFAG Gantries

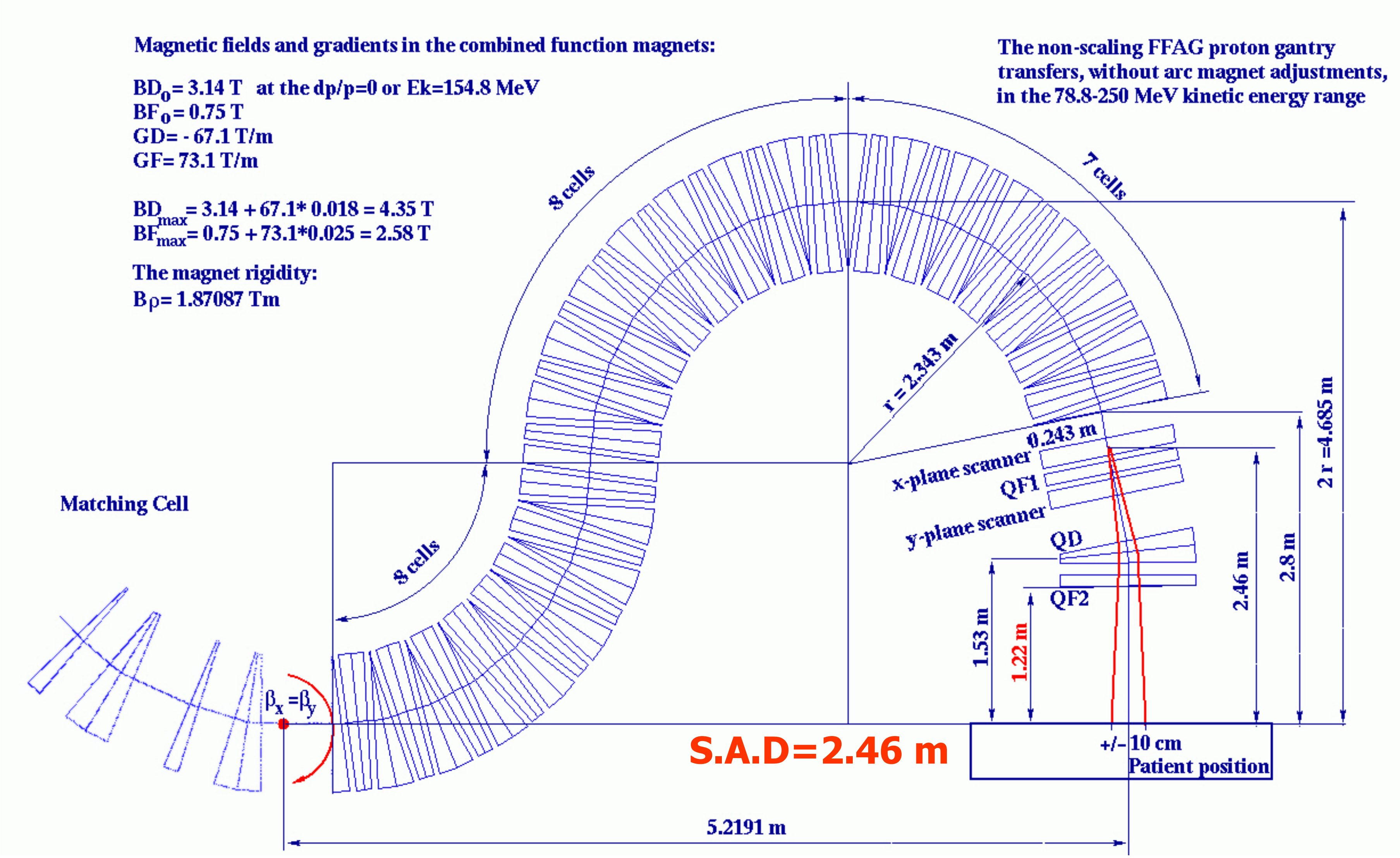

S.A.D=2.46 m

Courtesy of D. Trbojevic

FFAG: Large Momentum Acceptance

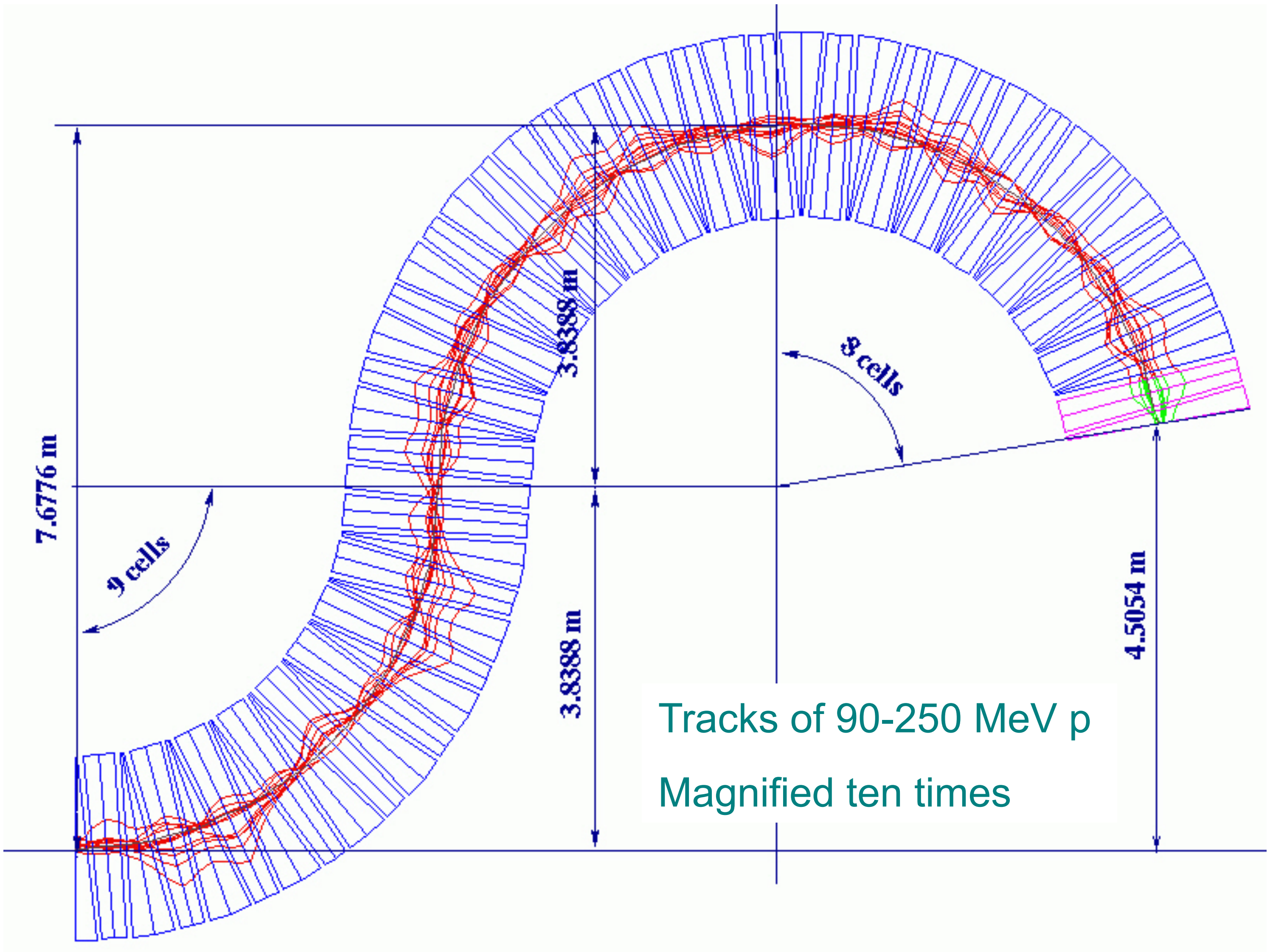

Courtesy of D. Trbojevic

Dielectric Wall Accelerators

- A recent new development in hadron therapy accelerators
  - Alternating fast-switching transmission lines – gradients up to 100 MV/m (!!)
  - Requires advanced materials
    - Very high-gradient insulators
    - High-frequency/voltage switches

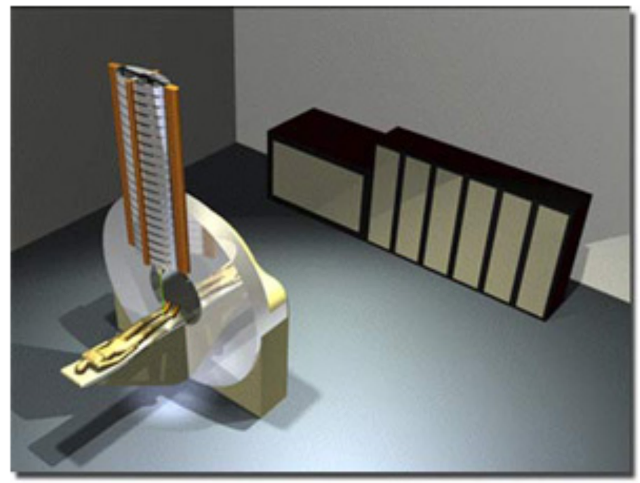

- ➢ In development by LLNL and Tomotherapy Group
- ➢ 10+ years from delivery

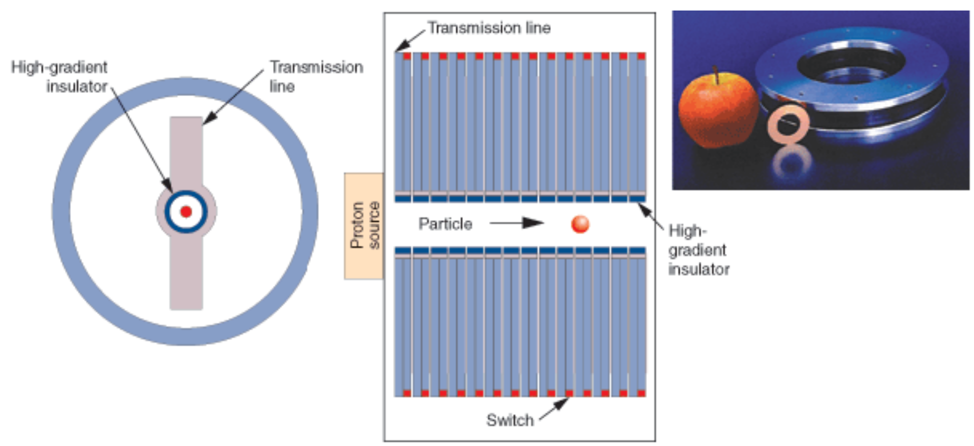

A compact dielectric wall accelerator is composed of a stack of rings made from thin, alternating layers of a metal and an insulator: (a) side view, (b) top view, and (c) sample ring. Transmission lines embedded in the rings produce the electric fields that propel charged particles along the tube. As the particles travel, a series of switches open and close, controlling the voltage applied to transmission lines in each section.

PET Imaging

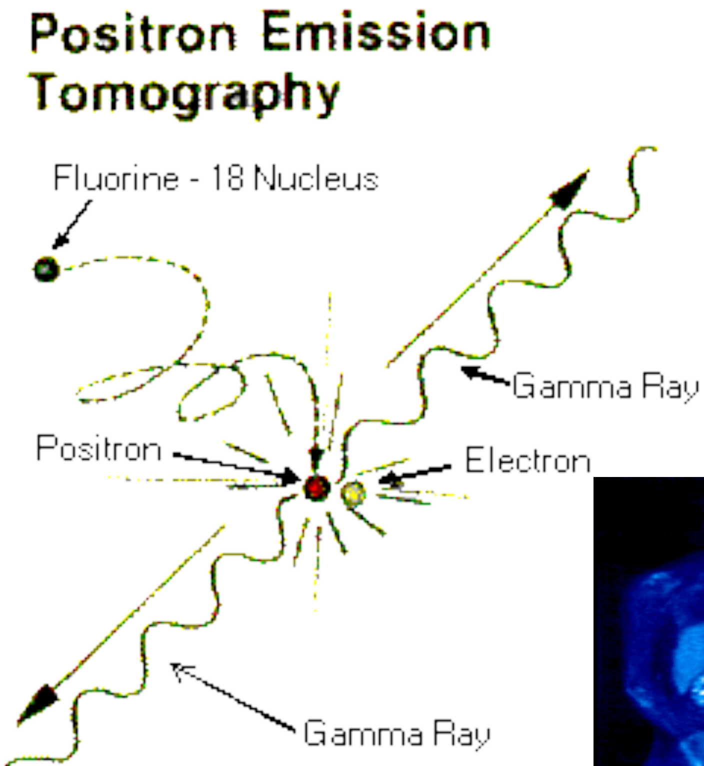

Metastasized prostate cancer

- PET: Positron Emission Tomography
  - Tag metabolically active compounds with positron emitters
    - e.g. ^{18}F deoxyglucose
  - Emitted positrons annihilate with nearby electrons producing back to back 511 keV gamma rays
  - Coincident gamma rays detected with photomultiplier tubes or avalanche photodiodes

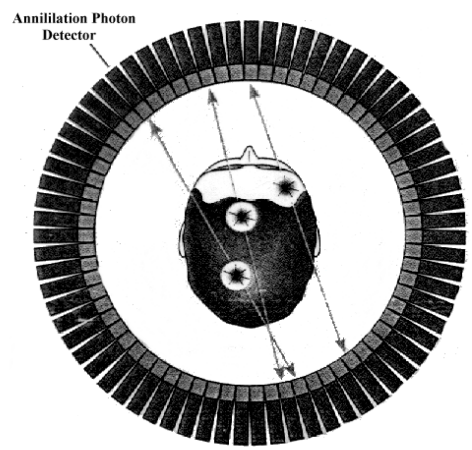

Radioisotopes for Medical Applications

- Use of radioisotopes is growing

Isotope	Target (% abund.) (type)	Energy (MeV)	Reaction
^{201}Tl	^{203}Tl (29.5) (S)	30 p	p,3n
^{123}I	^{124}Xe (0.094) (G)	30 p	p,2n
^{103}Pd	^{103}Rh (100) (S)	14 p	p,n
^{111}In	^{112}Cd (24.0) (S)	18 p	p,2n
^{225}Ac	^{225}Ra (S)	28 p	p,2n
^{186}Re	^{186}W (29.0) (S)	16 d	d,2n

Radioisotopes for Medical Applications

- New ones are being investigated
  - ^{123}Pd for treatment of prostate cancer
    - Half-life:17 days
    - 20 KeV x-ray
- Many useful radioisotopes with short lifetime are of interest but are not used because they would have to be produced close to their point of use
  - ^{68}Ga : labeling of biomolecules for PET imaging
    - $^{69}Ge(p,2n)\,^{68}Ga$, 68 mn
  - ^{64}Cu : cancer detection and treatment
    - $^{64}Ni(p,n)\,^{64}Cu$, 12.7 hr
  - ^{62}Cu (10 mn)
- Benefit could be obtained from many more radioisotopes with short half-life if they could be produced locally

Small Accelerators for Radioisotopes Production

Accelerator Parameters

Parameter	Value
Ions	p / d
Energy	5 – 40 MeV
Current	0.04 – 2 mA
Maintenance	Hands-On

•Current upgradeable to 4 mA

SARAF Project at Soreq Nuclear Research Center, Yavne, Israel

Small Accelerators for Radioisotopes Production

SARAF Project at Soreq Nuclear Research Center, Yavne, Israel

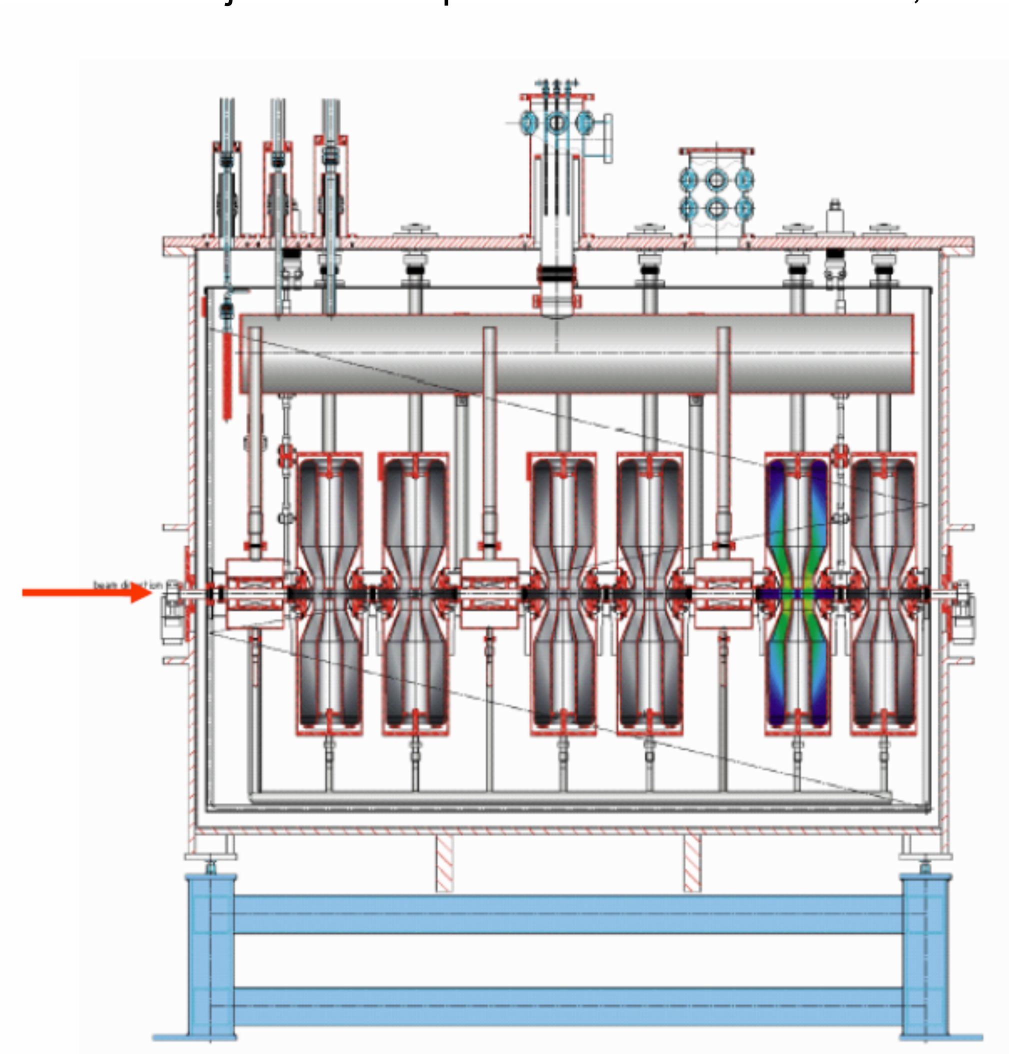

- The cryomodule houses six SC HWR cavities and three SC solenoids
- Separate beam and insulation vacuum
- Operating temperature 4.2°K
- six 2 kW solid state amplifiers
- Designed to accelerate 2 mA protons or deuterons beams

HWR Parameters	
Frequency	176 MHz
Optimal β (protons)	0.09
$L_{acc}=\beta\lambda$	0.15 m
ΔV @ E_{peak}	840 kV @ 25 MV/m
Q_0@E_{peak}	$>4.7\times10^8$
Cryogenic load	< 70 W
Q_{ext} Loaded BW	$\sim1.3\times10^6$ ~130 Hz

Small Accelerators for Medical and Other Applications

SARAF Project at Soreq Nuclear Research Center, Yavne, Israel